

2MASS PHOTOMETRIC REDSHIFT CATALOG: A COMPREHENSIVE THREE-DIMENSIONAL CENSUS OF THE WHOLE SKY

MACIEJ BILICKI^{1,2,*}, THOMAS H. JARRETT¹, JOHN A. PEACOCK³, MICHELLE E. CLUVER^{1,4} AND LOUISE STEWARD¹

¹Astrophysics, Cosmology and Gravity Centre, Department of Astronomy, University of Cape Town, Rondebosch, South Africa

²Kepler Institute of Astronomy, University of Zielona Góra, ul. Lubuska 2, 65-265 Zielona Góra, Poland

³Institute for Astronomy, University of Edinburgh, Royal Observatory, Edinburgh EH9 3HJ, UK

⁴Australian Astronomical Observatory, P.O. Box 915, North Ryde, NSW 1670, Australia

*Email: maciek(at)ast.uct.ac.za

Accepted to the Astrophysical Journal Supplement

ABSTRACT

Key cosmological applications require the three-dimensional galaxy distribution on the entire celestial sphere. These include measuring the gravitational pull on the Local Group, estimating the large-scale bulk flow and testing the Copernican principle. However, the largest all-sky redshift surveys – the 2MRS and IRAS PSCz – have median redshifts of only $z = 0.03$ and sample the very local Universe. There exist all-sky galaxy catalogs reaching much deeper – SuperCOSMOS in the optical, 2MASS in the near-IR and WISE in the mid-IR – but these lack complete redshift information. At present, the only rapid way towards larger 3D catalogs covering the whole sky is through photometric redshift techniques. In this paper we present the 2MASS Photometric Redshift catalog (2MPZ) containing 1 million galaxies, constructed by cross-matching 2MASS XSC, WISE and SuperCOSMOS all-sky samples and employing the artificial neural network approach (the ANN $_z$ algorithm), trained on such redshift surveys as SDSS, 6dFGS and 2dFGRS. The derived photometric redshifts have errors nearly independent of distance, with an all-sky accuracy of $\sigma_z = 0.015$ and a very small percentage of outliers. In this way, we obtain redshift estimates with a typical precision of 12% for all the 2MASS XSC galaxies that lack spectroscopy. In addition, we have made an early effort towards probing the entire 3D sky beyond 2MASS, by pairing up WISE with SuperCOSMOS and training the ANN $_z$ on GAMA redshift data reaching currently to $z_{\text{med}} \sim 0.2$. This has yielded photo- z accuracies comparable to those in the 2MPZ. These all-sky photo- z catalogs, with a median $z \sim 0.1$ for the 2MPZ, and significantly deeper for future WISE-based samples, will be the largest and most complete of their kind for the foreseeable future.

Keywords: catalogs – (cosmology:) large-scale structure of universe – galaxies: distances and redshifts
– methods: data analysis – methods: statistical – surveys

1. INTRODUCTION

Observational studies of the large-scale structure in the Universe have made great progress in recent years through such projects as the 2dF Galaxy Redshift Survey (2dFGRS, Colless et al. 2001), the Sloan Digital Sky Survey (SDSS, Eisenstein et al. 2011) and the 6dF Galaxy Survey (6dFGS, Jones et al. 2004). These and other current and near-future redshift surveys have been highly successful in extracting cosmological information from the properties of the cosmic web.

Despite these achievements, some aspects of large-scale structure studies still require major improvements on the observational side. In particular, we lack a dense, deep and uniform three-dimensional catalog of galaxies that covers the whole sky. Currently the two largest all-sky catalogs of this type are the IRAS Point Source Catalog Redshift Survey (PSCz, Saunders et al. 2000) and the 2MASS Redshift Survey (2MRS, Huchra et al. 2012), based respectively on the observations made with the Infrared Astronomical Satellite (Neugebauer et al. 1984) and the ground-based Two Micron All Sky Survey (Skrutskie et al. 2006). The PSCz contains more than 15,000 IRAS-selected galaxies (with fluxes larger than 0.6 Jy in the 60 μm band), covers 84% of the sky and has a median redshift of $z = 0.026$. The 2MRS is larger and denser, but slightly shallower (in terms of

an effective depth), containing over 43,000 galaxies with K_s -band magnitudes below 11.75, distributed over 91% of the sky and with a median redshift of $z = 0.028$. The number of galaxies and the depth of these surveys are an order of magnitude smaller than in the currently largest three-dimensional low-redshift surveys, such as the 2dFGRS or SDSS; see table 1 in Huchra et al. (2012) for a comparison of recent and historic catalogs, and Figure 1 herein for redshift distributions of several surveys of the nearby Universe. An important additional remark is that even these ‘all-sky’ surveys are highly incomplete for the swath of the sky that is obscured by the foreground Milky Way, the so-called Zone of Avoidance (ZoA). In the case of the near-infrared 2MRS, for which the Galactic extinction is not as significant as in the optical, it is source confusion and stellar crowding that limits the detection of galaxies behind the Milky Way (Jarrett et al. 2000a; Kraan-Korteweg & Jarrett 2005).

Comprehensive all-sky redshift surveys are challenging: a sample that covers the entire celestial sphere and remain uniform in terms of photometry and other observable properties requires either a single space-borne instrument or twin ground-based telescopes. Converting this into a three-dimensional all-sky sample of galaxies requires subsequent cross-matching with existing redshift surveys and spectroscopic follow-up for those sources that have no redshift information (see e.g. Huchra et al.

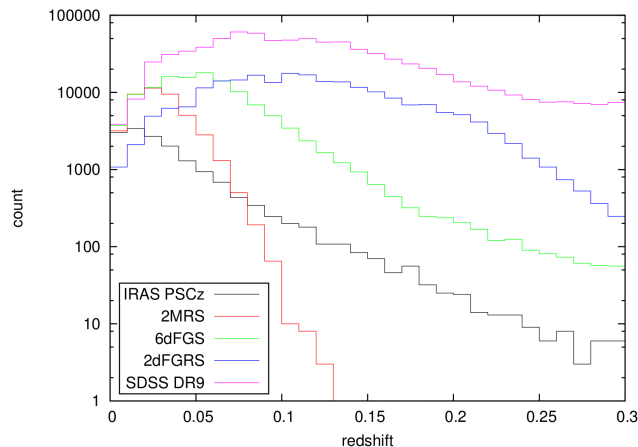


Figure 1. Redshift distribution of the most important galaxy surveys of the low-redshift Universe. Only the two shallowest of these, namely 2MRS and PSCz, cover (almost) the entire sky. Note the logarithmic scaling of the y -axis.

2012). Currently no such all-sky redshift surveys in the optical or infrared bands are being performed or even envisaged: for instance, the forthcoming major cosmological space mission of the European Space Agency, Euclid (Laureijs et al. 2012), which aims at imaging a billion galaxies and measuring nearly 50 million galaxy redshifts, will cover $\sim 15,000$ deg². Another promising concept, known as TAI PAN (Colless et al. 2013), will follow up the 6dFGS using the UK Schmidt Telescope, with a 2-magnitude deeper redshift survey matched to the catalogs of WISE and VISTA-VHS; but again, would not cover the entire sky, unless it is extended to the North, with the use of an additional instrument. Thus sadly the PSCz and 2MRS are likely to remain the deepest complete catalogs of their kind for many years. Beyond the optical and infrared domains, the future radio surveys show promise to achieve all-sky redshift coverage: the WALLABY *HI* survey, planned for the Australian SKA Pathfinder (ASKAP, Johnston et al. 2008), and its Northern counterpart, APERTIF (Verheijen et al. 2009) using the Westerbork Radio Telescope in the Netherlands.

The principal aim of the present paper is to show that by combining the largest *photometric* all-sky galaxy catalogs we obtain reliable and unbiased photometric redshifts over the entire celestial sphere, reaching currently a median $z \sim 0.1$ and at least double this in the near future, with reasonably small and well-behaved errors. The key is to use uniform photometric measurements spanning from the optical to the mid-infrared. Such data are available through 2MASS, WISE and SuperCOSMOS all-sky samples. Of these three surveys, 2MASS is the shallowest, so accordingly we based our analysis on the 2MASS Galaxy Catalog (Jarrett et al. 2000b). Thanks to the multi-wavelength coverage, we were able to efficiently apply the artificial neural network approach (the ANNz algorithm), trained on such redshift surveys as discussed above and thoroughly tested in selected fields, finally constructing the 2MASS Photometric Redshift catalog (2MPZ). In addition, we briefly consider the prospects of probing deeper than allowed by the 2MASS sample, by using a combination of WISE and optical imaging.

The paper is organized as follows. In Section 2 we

present the motivations for obtaining deeper all-sky redshift surveys. Section 3 summarizes efforts to date regarding all-sky photometric redshift catalogs. In Section 4 we describe the photometric and redshift surveys used within our project. A discussion on the photometric redshift methods, including the one we adopted here, is given in Section 5. Section 6 presents tests of photometric redshift estimation in selected fields. A description of the all-sky 2MASS Photometric Redshift catalog follows in Section 7. We conclude and present future prospects in Section 8.

2. THE NEED FOR ALL-SKY GALAXY SURVEYS

Several cosmological problems call for all-sky three-dimensional surveys of at least a comparable depth to that of the SDSS main galaxy sample or 2dFGRS. Firstly, with the advent of precision cosmology it has become important to probe *observationally* the degree of the homogeneity and isotropy of the late Universe (Clarkson 2012), as these two properties, the Copernican Principle (CP), underlie the standard cosmological model. Although tests applicable to surveys of even limited sky coverage exist (e.g. Hogg et al. 2005; Sarkar et al. 2009; Gibelyou & Huterer 2012; Marinoni et al. 2012; Scrimgeour et al. 2012), their usefulness for all-sky redshift surveys is currently limited by the shallowness of the latter.

Secondly, some important cosmological studies – many of which also probe the CP in the low-redshift Universe, even if indirectly – can be performed only with the use of an all-sky redshift survey. For instance, such a catalog is essential to examine the amplitude and the scale of convergence of the gravitational acceleration of the Local Group, via the so-called clustering dipole in galaxy distribution (e.g. Bilicki et al. 2011, and references therein). Although this measurement is possible, in principle, with the use of a ‘2.5-dimensional’ catalog (i.e. with galaxy positions and fluxes only), redshift information is then essential for determination and characterization of the attractors and vital when comparing with theoretical expectations of particular cosmological models (Juszkiewicz et al. 1990; Lahav et al. 1990). The issue of the dipole convergence or lack thereof, as well as of the sources of the pull on the Local Group, still remains contentious, due to the lack of sufficiently deep and dense all-sky redshift surveys (see e.g. Basilakos & Plionis 2006; Erdoğan et al. 2006; Kocevski & Ebeling 2006; Lavaux et al. 2010), as well as paucity of information in the ZoA, where many attractors are known or suspected to lie (e.g. Woudt et al. 2008).

Next, as was shown by Nusser et al. (2011) and more recently applied by Branchini et al. (2012), an all-sky redshift catalog with uniform photometry can be used to place constraints on the amplitude and direction of the large-scale bulk flow, i.e. net peculiar motions of galaxies in a sphere centered on the Local Group, on scales larger than currently available. Such a measurement traditionally requires catalogs of peculiar velocities (see e.g. Nusser & Davis 2011; Turnbull et al. 2012, for recent contributions), which are both limited to the very local Universe ($z < 0.02$) and compromised by large uncertainties in distance indicators used. In order to probe beyond the reach of peculiar velocity catalogs, i.e. $\gtrsim 100$ Mpc, galaxy clusters are being used, notably through the kine-

matic Sunyaev-Zel'dovich effect (kSZ, Sunyaev & Zel'dovich 1980). Nevertheless, the attempts to measure this effect still yield relatively low signal-to-noise, resulting in conflicting estimates of the bulk flows from this method, including claims of excessively high amplitudes on very large scales (e.g. Kashlinsky et al. 2008; Planck Collaboration et al. 2013b).

A similar idea to the one discussed above lies behind the method of Nusser et al. (2012) to probe the growth rate parameter f , combined with the linear bias b into $\beta \equiv f(\Omega)/b$, at the effective redshift of a survey, independently of redshift-space distortions (Beutler et al. 2012) or velocity-velocity comparisons (Davis et al. 2011). Using $\sim 45,000$ 2MRS galaxies, Branchini et al. (2012) were able to obtain $\sim 25\%$ accuracy on β ; this error should decline as $N^{-1/2}$ for larger samples. Again, uniform and accurate photometry, large number of galaxies and wide-angle sky coverage are crucial for this approach.

Finally, the widest possible angular coverage of the redshift survey is desirable in those analyses where cross-correlation between the low-redshift large-scale structure (LSS) and cosmic microwave background (CMB) temperature distribution is explored. The most widely studied in this respect is the integrated Sachs-Wolfe effect (ISW, Sachs & Wolfe 1967) – an important cosmological probe, as its detection gives confirmation of dark energy in the late Universe. The all-sky surveys used for the ISW measurements include 2MASS (Afshordi et al. 2004; Rassat et al. 2007; Francis & Peacock 2010) and the Wide-field Infrared Survey Explorer (WISE, Kovács et al. 2013); but the significance of ISW detection from these and other analyses is still weak, and deeper wide-angle redshift surveys would be valuable. Another possible application of an all-sky redshift survey is the gravitational lensing of the CMB by the LSS; see for instance the recent analysis by the Planck team (Planck Collaboration et al. 2013a) and the strong cross-correlation with WISE quasars measured by Geach et al. (2013).

3. ALL-SKY PHOTOMETRIC REDSHIFTS

Currently the only rapid route to an all-sky three-dimensional catalog that would be significantly deeper than 2MRS or PSCz is to use a broad-band photometric survey, such as 2MASS, gather all available spectroscopic redshifts for its galaxies (from other surveys) and estimate *photometric redshifts* for the remaining objects. The technique of photometric redshifts (e.g. Benítez 2000; Bolzonella et al. 2000, and references therein) is now widely used: e.g., the MegaZ-LRG sample of ~ 1.5 million luminous red galaxies from the SDSS DR6 (Abdalla et al. 2011) is one of many prominent examples of a successful application.

In the present paper we describe our successful efforts towards obtaining the deepest three-dimensional catalog of galaxies covering the entire sky, based mainly on 2MASS and its near-infrared measurements of resolved sources. Using this sample for such a purpose is not a new idea: almost a decade ago Jarrett (2004) used the three-band near-infrared photometry of 2MASS to estimate in a simple way luminosity distances to galaxies (the 2MASS XSCz). This method assumes that all galaxies have similar luminosities (L^*) and what modifies their near-infrared colors is the cosmic reddening. The measured integrated flux was the primary compo-

nent, while the near-infrared colors added secondary information. This technique, being very crude in terms of accuracy (20 to 30%), still provided a means to generate qualitative maps of the spatial distribution of galaxies and thereby construct an all-sky ‘big picture’ view of the local Universe¹.

The XSCz method was particularly suitable to reveal clusters of galaxies as the redshift uncertainty of this approach declines with the square root of the number of cluster members seen by 2MASS. The photometric redshifts of galaxy clusters as estimated by Jarrett (2004) using only 2MASS photometry were typically accurate to 20%, or worse for individual sources, and it was concluded that near-infrared colors alone are not sufficient as a discriminant of galaxy redshifts. Such photo- z 's are ultimately constrained by the fact that the 2MASS J , H and K_s bands are, on the one hand, notably sensitive to the photospherically emitted light from evolved stars (e.g., K giants), and hence able to track the cosmological k -correction of this light out to low ($z < 0.2$) redshifts, but on the other hand insensitive to star forming, low-surface brightness and dwarf galaxies, resulting in color redundancies that are difficult to track with redshift. As we emphasize in the present paper, the solution is to add more photometric bands, at least one in the optical and one in the mid-infrared.

Another approach to obtain an all-sky 3D catalog based on 2MASS was taken by Francis & Peacock (2010). Working in the context of analyzing the ISW signal, they derived photometric redshift estimates by matching the 2MASS data with optical catalogs generated from SuperCOSMOS scans of major photographic sky surveys (Hambly et al. 2001c). A five-band $BRJHK$ photometric data set was used, calibrated via spectroscopic redshifts for about 30% of the galaxies, thanks to SDSS, 2dFGRS and 6dFGRS. This yielded photometric redshifts with an rms dispersion of about 0.033. Even better results can be achieved by adding further optical/UV photometry such as the SDSS (Wang et al. 2008, 2009) or additionally the Galaxy Evolution Explorer (GALEX, Way & Srivastava 2006; Way et al. 2009), although this is only possible over a fraction of the sky.

In this present work, we show that by combining the 2MASS XSC with optical data from SuperCOSMOS and mid-infrared from WISE, and using the powerful machine-learning neural network method, photometric redshifts are very significantly ameliorated, to an rms error of around 0.015, and any overall biases are correspondingly reduced. We therefore greatly improve on these earlier attempts concerning all-sky 3D catalogs based on the 2MASS sample, which results in generating the 2MASS Photometric Redshift catalog, as well as examining the possibility to go beyond the reach of this survey. Both are feasible thanks to the release of the data from the Wide-field Infrared Survey Explorer (WISE, Wright et al. 2010), as well as increasing numbers of spectroscopic redshifts from such surveys as SDSS and the Galaxy And Mass Assembly (GAMA, Driver et al. 2009).

¹ See e.g. <http://www.ast.uct.ac.za/~jarrett/lss/> for some whole-sky visualizations.

4. PHOTOMETRY AND REDSHIFTS USED

4.1. 2MASS XSC

The basic photometric dataset used in our study is the *Two Micron All Sky Survey Extended Source Catalog* (2MASS XSC; Jarrett et al. 2000b). 2MASS (Skrutskie et al. 2006) was a ground-based survey between 1997 and 2001, covering 99.998% of the celestial sphere and delivering uniform, precise photometry and astrometry over the entire sky in the near-infrared J ($1.25 \mu\text{m}$), H ($1.65 \mu\text{m}$), and K_s ($2.16 \mu\text{m}$) bandpasses. Observations were conducted from two dedicated 1.3 m diameter telescopes located at Mount Hopkins, Arizona, and Cerro Tololo, Chile. The 2MASS All-Sky Data Release includes 471 million source extractions in the Point Source Catalog, and over 1.6 million resolved objects in the Extended Source Catalog. Of the latter, more than 98% are galaxies, and the remaining objects are mainly Galactic diffuse sources (Jarrett 2004). The 2MASS XSC was designed to satisfy the survey science requirements as outlined by Jarrett et al. (2000b), the most important being the reliability and completeness for unconfused regions of the sky. These were met for sources brighter than $K_s = 13.5$ (~ 2.7 mJy) and resolved diameters of galaxies above ~ 10 – $15''$. Until the advent of WISE, the 2MASS XSC was the largest all-sky astro- and photometric catalog of galaxies, and currently retains this status where extended-source photometry is concerned.

The complete 2MASS Extended Source Catalog contains 1,646,966 entries; however, a small fraction of these are artifacts, have erroneous or null measurements. We have removed from our sample the sources that fulfill any of the following criteria: flag `vc=2` (non-extended Galactic sources, usually blends of stars, confirmed visually; 7383 objects); flag `cc_flag=a` (artifacts, 122 sources); J , H or K_s band magnitude(s) NULL or excessively high (erroneous) – over 170,000 objects, lacking measurements mainly in the H and J bands. This gave us 1,471,442 sources for further analysis (the ‘2MASS good’ sample). As the basic photometry we use the 20 mag arcsec $^{-2}$ isophotal fiducial elliptical aperture magnitudes (`j/h/k.m.k20fe`) together with relevant error estimation (1-sigma uncertainty for these magnitudes). The magnitudes were corrected for Galactic extinction with the use of the Schlegel et al. (1998) maps (SFD) and the $A_\lambda/E(B - V)$ coefficients taken from Cardelli et al. (1989).

Galactic extinction is generally not an important factor for the infrared window, however, the zone within 5° of the Galactic Plane is susceptible to extinction errors and coefficient uncertainties, rendering potential systematics in the 2MASS photometry at these low Galactic latitudes. We note that due to overestimation of the extinction by the SFD maps within $|b| < 5^\circ$ (e.g. Schröder et al. 2007), many of the sources therein are corrected improperly and they were further removed due to unreliable magnitudes, often reaching negative values. For those reasons, the strip of $|b| < 5^\circ$, and $|b| < 8^\circ$ or even wider around the Bulge ($\ell > 330^\circ$ and $\ell < 30^\circ$), is usually masked out in all-sky cosmological applications of 2MASS data (cf. Maller et al. 2003; Bilicki et al. 2011). In addition, issues are being raised regarding the SFD maps in general, for instance that they may overestimate the extinction over the entire sky, not only in the Galactic

Plane (Schlafly & Finkbeiner 2011; Yuan et al. 2013) and new dust maps are currently in development, in particular with the use of WISE data (Meisner & Finkbeiner 2013). This recalibration, once available, will however not be significant for the majority of 2MASS sources, but will be an important factor with the optical corrections.

Finally, an important remark is that for any cosmological analyses such as those mentioned in Section 1, which require both uniformity and completeness over the entire sky, only a part of the total ‘2MASS-good’ sample will be applicable. The completeness limit of 2MASS (in terms of extragalactic source counts) is ~ 13.9 in the K_s band (Jarrett 2004) and galaxies beyond this magnitudes are usually removed whenever all-sky uniformity is needed (e.g. Bilicki 2012). There are approximately 1 million 2MASS-good galaxies with extinction-corrected magnitudes $K_s < 13.9$, covering 96% of the sky, i.e. basically the entire celestial sphere, except for the Galactic bulge area (e.g. Gibelyou & Huterer 2012). See also the latter reference, as well as Maller et al. (2003) and Jarrett (2004), for detailed plots of all-sky 2MASS XSC distribution. The mean source density in the areas where the 2MASS sample is complete amounts to ~ 26 deg $^{-2}$.

4.2. WISE

For the purposes of our project, the photometric data from 2MASS were supplemented by the measurements made within the WISE and SuperCOSMOS surveys. The former, the *Wide-field Infrared Survey Explorer* (Wright et al. 2010), is a space-borne telescope that in 2010 mapped the entire sky at 3.4, 4.6, 12 and 22 μm ($W1 - W4$). WISE achieved 5σ point source sensitivities better than 0.08, 0.11, 1 and 6 mJy in unconfused regions on the ecliptic in the four bands (but is considerably deeper at the ecliptic poles due to its polar orbit; see Jarrett et al. 2011), which is a major advance when compared to the now historical IRAS survey, as well as to the contemporary AKARI mission (Murakami et al. 2007), yet another orbital survey of the whole sky in the infrared. The all-sky WISE release (Cutri & et al. 2012) includes all the data taken during the WISE full cryogenic mission phase that were processed with improved calibrations and reduction algorithms. The released data products contain a Source Catalog with positional and photometric information for over 563 million objects detected on the WISE images. A large fraction of these (well offset from the Galactic Plane) are galaxies, which makes WISE significantly deeper than 2MASS. The full potential of WISE extragalactic science remains to be explored: for instance, a ‘WISE XSC’, which will incorporate aperture photometry of resolved (extended) sources, is now under construction (see discussion in Jarrett et al. 2013). A particular example of early WISE XSC results is the WISE-GAMA catalog presented in Cluver et al. (2013, in prep.).

Except for the case of the GAMA fields (see Subsection 6.4), our basic photometric catalog is the 2MASS XSC. As we aim at as high a matching rate with WISE as possible, from the latter we use only the photometry in its two shortest wavelengths: $W1$ and $W2$ (although future updates may include $W3$ measurements as well). We expect that the galaxies present in 2MASS should always be seen in these shorter WISE bands, which have a much higher detection rate than the two other bands, $W3$ and

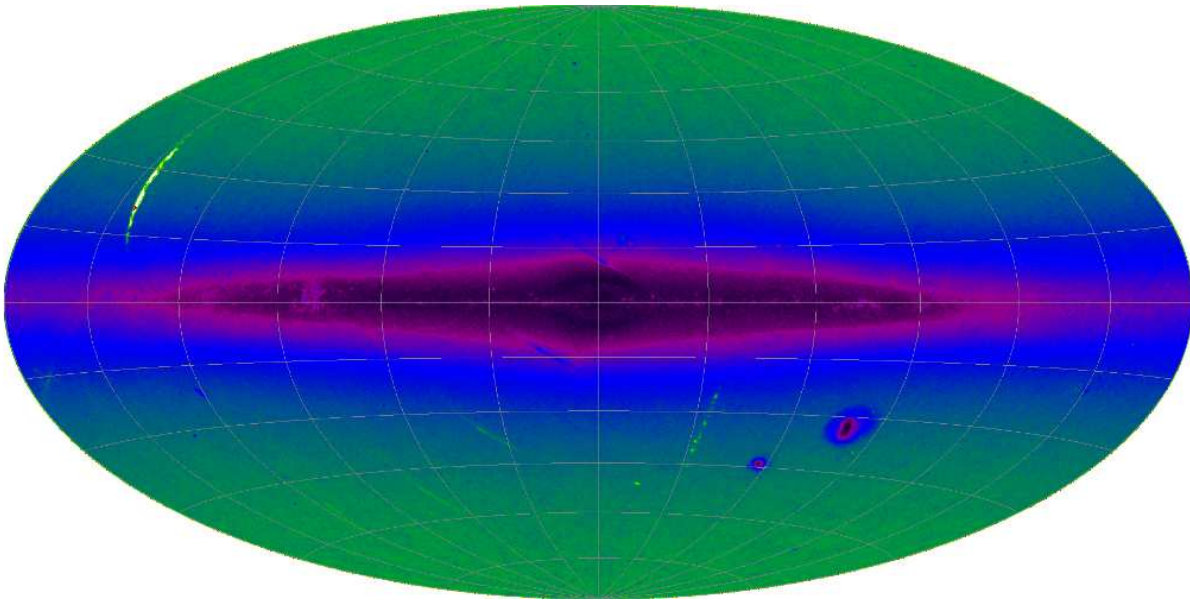


Figure 2.

Aitoff projection, in Galactic coordinates, of all-sky source distribution in the WISE catalog, flux-limited at 15.5 in the $W1$ band (more than 230 million objects in the plot). This figure includes both extended and point-like sources.

$W4$ (Cutri et al. 2012). The overwhelming majority of all the objects in the WISE catalog have detections in the $W1$ band, and this rate is still fairly high for $W2$ (for $> 2\sigma$ detections it is respectively 99.1% and 83.5% of the total). The matching rate of the ‘2MASS-good’ sample with WISE $W1$ - and $W2$ -detected sources amounts in general to over 99%. We pre-filtered the WISE catalog data by demanding that `cc_flags[?] ≠ ‘DPHO’` (no known artifacts; ‘?’ stands for 1 or 2), `w?sat` ≤ 0.1 (no more than 10% of saturated pixels) and `w?snr` ≥ 5 (sufficiently high profile-fit measurement signal-to-noise ratio – equivalent to an upper limit on magnitude errors of 0.21). Figure 2 presents an Aitoff Galactic projection of all WISE sources brighter than $W1 = 15.5$, pre-filtered as described above. There are over 230 million detections shown in this plot, of which 67 million are located at high Galactic latitudes of $|b| > 20^\circ$. Note however that the WISE catalogs always contain a significant fraction of stars, even far away from the Galactic Plane (Jarrett et al. 2011), and especially at bright magnitudes. Apart from the Galactic Plane (with mostly stars), some other features clearly stand out: the Magellanic Clouds; lack of measurements in a strip with $\ell_{\text{Gal}} \simeq 140^\circ$ and $15^\circ < b < 35^\circ$ due to ‘torque rod gashes’² or some incompleteness due to moon contamination (see discussion in Kovács et al. 2013). We note that some of these biases are mitigated after matching WISE with the 2MASS XSC up to the completeness limit of the latter, as the resulting dataset is about 1.5 magnitudes shallower than the one in Figure 2. Additionally, the forthcoming post-cryo all-sky WISE release (‘ALLWISE’), as well as a proper ‘WISE XSC’, will alleviate at least some of these problems.

The basic photometry in WISE is given by the `w?mpro` magnitudes measured with profile fitting appropriate for point sources. However, as emphasized in Jarrett et al. (2013) and in the Cautionary Notes of the WISE Ex-

planatory Supplement³, the Catalog contains both point-like and resolved sources, so the profile-fitting photometry underestimates the true brightness of extended objects. Our most recent findings show that probably all the 2MASS XSC galaxies are also resolved by WISE (Jarrett et al., in prep.) – but extended-source photometry is currently available only for a fraction of them. Specifically, those WISE objects that are located within the 2MASS XSC perimeter – defined to be the K_s -band isophotal circular diameter inflated by 10% – and have a radial distance between the WISE and 2MASS source of $< 2''$, have integrated WISE fluxes measured in the elliptical aperture with a size, shape and orientation that is scaled from that of an associated 2MASS XSC source. These integrated magnitudes are given as `w?gmag` in the database and in principle could serve as a proxy for WISE galaxy fluxes before a proper extended source catalog is available for this survey. However, as only about half of all 2MASS-good sources have `w?gmag` measurements, we decided not to use this type of photometry in order to avoid biases in the photometric redshifts due to mixing extended- and point-source fluxes. Instead, until proper resolved source photometry is made available for the whole WISE catalog, we continue to use the `w?mpro` magnitudes, automatically correcting profile-fit photometry for extended emission using differential aperture photometry information from $5.5''$ and $11''$ circular aperture measurements, `w1mag_1–w1mag_3` (Cutri et al. 2012). This one additional parameter used as an input for the neural networks enables them to ‘learn’ how to compensate for the flux lost due to the imposed assumption of a point source.

All the WISE $W1$ and $W2$ magnitudes were extinction-corrected using coefficients according to Flaherty et al. (2007): $A_{W1}/EBV = 0.231$ and $A_{W2}/EBV = 0.194$.

² http://wise2.ipac.caltech.edu/docs/release/allsky/expsup/sec6_2.html#lowcoverage

³ http://wise2.ipac.caltech.edu/docs/release/allsky/expsup/sec1_4.html

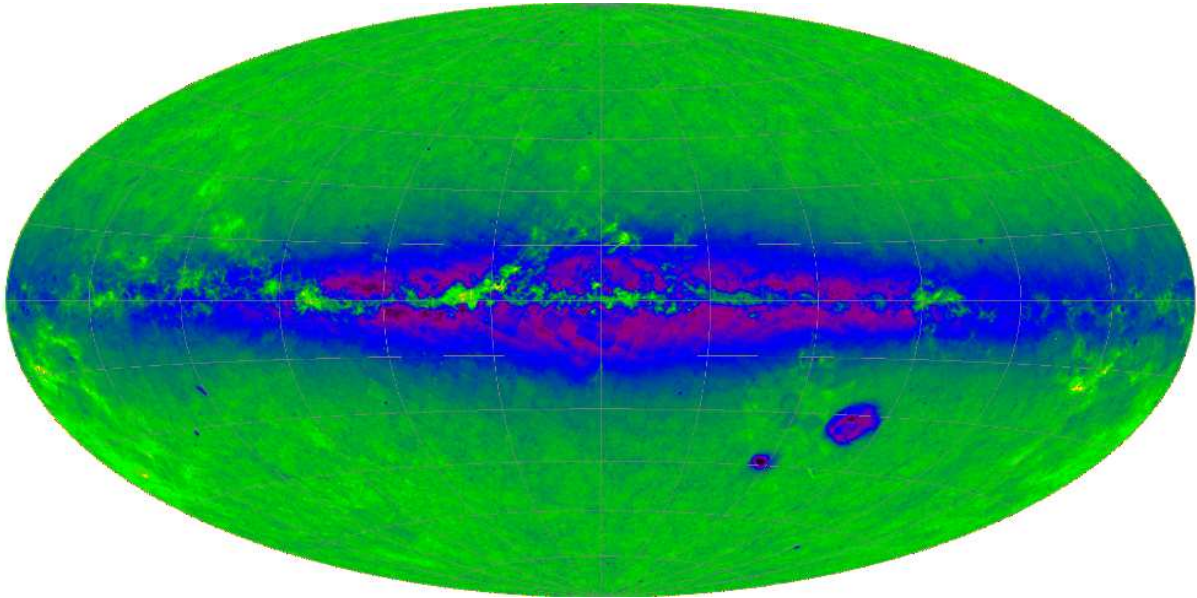


Figure 3.

Aitoff projection of all-sky extended source distribution in the SuperCOSMOS survey, in Galactic coordinates. Objects below a limiting magnitude of $B = 21$ are shown (almost 189 million detections). The spurious overdensities around the Milky Way and in the Magellanic Clouds arise from blending.

4.3. SuperCOSMOS

The *SuperCOSMOS Sky Survey* (SSS) program (Hambly et al. 2001c,b,a) was a project to digitize the photographic measurements of the sky in three band (optical BRI), via automatic scans of sky atlas photographs. The source photographic material came from the United Kingdom Schmidt Telescope (UKST) in the south and the Palomar Observatory Sky Survey-II (POSS-II) in the north, observations having been taken during the last quarter of the twentieth century. These catalogs were given an accurate photometric calibration with the use of SDSS photometry, overlaps of plates and by requiring uniformity in average color between the optical and 2MASS J bands (Francis & Peacock 2010); the details of the procedure will be described in Peacock et al. (in prep.). Given suitable calibration information, these photographic plates are capable of yielding impressively accurate and uniform photometry. A good model for the rms residual between SuperCOSMOS photometry and SDSS predictions is obtained by adding in quadrature a constant value of 0.06 and a magnitude-dependent $0.2 \times 10^{0.4(m-m_{\text{lim}})}$, where m_{lim} is the relevant 5σ completeness limit. The depth fluctuates between different plates, but typical figures for m_{lim} are approximately $B = 22$, $R = 21$, $I = 19.5$.

The SuperCOSMOS magnitudes were given a zero point in which they would coincide with SDSS photometry in the case of an object with the colors of the fundamental SDSS standard. They are thus not a true AB system: see Peacock et al. (in prep.) for the color equations. As the passbands for the UKST and POSS-II were slightly different, in the magnitudes provided in the SuperCOSMOS database there is in effect a small color-dependent offset between the North and the South (i.e. above and below $\delta_{1950} = 2.5^\circ$). By comparison with SDSS, we designed the following direct corrections to compensate for this effect and match the measurements in the two hemispheres, applied to the data from the

South ($\delta_{1950} < 2.5^\circ$):

$$B_S^{\text{corr}} = B - 0.03(B - R)^2 + 0.03(B - R) - 0.01 \quad (1)$$

$$R_S^{\text{corr}} = R - 0.04(B - R)^2 + 0.08(B - R) - 0.02 \quad (2)$$

$$I_S^{\text{corr}} = I - 0.02(R - I)^2 - 0.07(R - I) + 0.01 \quad (3)$$

where the subscript "S" refers to the south and right-hand sides include values taken directly from the catalog. Also the extinction-correction was hemisphere-dependent: we used $A_B^N = 4.165$ and $A_R^N = 2.773$ in the North, $A_B^S = 4.011$ and $A_R^S = 2.778$ in the South, and $A_I = 2.016$ for the entire sky. In order to remove any residual biases not compensated for by this calibration, in the photometric redshift estimation process we trained separate neural networks for the two hemispheres.

The SuperCOSMOS data (SCOS for short) are curated at <http://surveys.roe.ac.uk/ssa/>, where multicolor information is provided for 1.9 billion sources, and extended source photometry is given whenever the object has been classified as such (gCorMags in the database). We used only sources with `meanClass = 1` (source classified as a galaxy) and quality flags in the relevant bands below 2048 (no strong warnings, nor severe defects, Hambly et al. 2001b). In Figure 3 we plot the all-sky density map of SCOS extended sources, limited to observed $B < 21$, which is one magnitude less than the estimated completeness limit. At these depths, there are almost 189 million sources with B and R extended-source photometry measured over the whole sky, although only those away from the Galactic Plane are applicable for extragalactic studies. For instance, there are over 50 million SCOS extended sources with $B < 21$ at Galactic latitudes of $|b| > 20^\circ$, which are mostly extragalactic. Here, unlike in the case of WISE, the increased density of detections near the Plane is due to spurious extended sources arising from blending of stars.

4.4. Spectroscopic redshifts of 2MASS galaxies

About one third of all 2MASS galaxies already have spectroscopic redshifts, although their coverage on the sky remains far from uniform. In a study related to the discussion in this Subsection, Lavaux & Hudson (2011) presented the situation as it was in mid-2011, by compiling what they dubbed the *2M++ catalog*, which included 69,160 2MASS-selected galaxies, reaching depths up to $K_s \leq 12.5$ (although the effective depth varied on the sky). Their primary sources of redshifts were an early version of the 2MRS ($K_s \leq 11.25$), the 6dFGS and the SDSS Data Release 7. Compiling the 3D data of the sources was only the starting point for Lavaux & Hudson (2011), as they also assessed completeness in redshift for each of the regions and proposed the weights and corrections for incompleteness in redshift, sky coverage (Zone of Avoidance), as well as in apparent magnitude limits. Additionally, they presented the density field for their survey, and discussed the importance of large-scale structures such as the Shapley Concentration. In contrast, we prefer to recover individual photometric redshifts based on the *observed* properties of our sources. This avoids the need for corrections such as ‘redshift-cloning’ to mitigate small-scale redshift incompleteness arising from fiber collisions, as well as adjustment of apparent galaxy magnitudes due to the effects of cosmological surface brightness dimming and stellar evolution. The latter *depend* on the redshift of the source and must not be applied if the photometric redshift technique is to work properly.

We compiled our primary spectroscopic redshift sample for 2MASS galaxies from the publicly available datasets described below. We used heliocentric redshifts throughout, because to work in the CMB frame it would be necessary to apply a Doppler k -correction to the photometry, which is redshift-dependent. Additionally, negative recession velocities in the heliocentric frame (although real for a tiny fraction of galaxies located within the Local Volume) are not of interest for our project and such sources are skipped.

The redshift surveys compiled within our project were the following:

- 2MASS Redshift Survey (2MRS, Huchra et al. 2012), a uniform all-sky (except for the ZoA) sample that contains 44,599 2MASS-selected galaxies with $K_s \leq 11.75$ and $|b_{\text{Gal}}| \geq 5^\circ$ ($\geq 8^\circ$ toward the Galactic bulge); of these, 43,361 are present in the ‘2MASS good’ sample and have positive heliocentric redshifts;
- Sloan Digital Sky Survey Data Release 9 (SDSS DR9, Ahn et al. 2012), which includes 1,685,470 galaxy and quasar redshifts, mainly in the North Galactic Cap ($b_{\text{Gal}} > 20^\circ$), with some patches in the southern Galactic hemisphere; there are 324,737 of these sources in the ‘2MASS good’ sample, with $z_{\text{hel}} > 0$;
- 6dF Galaxy Survey Data Release 3 (6dFGS DR3, Jones et al. 2009), a 2MASS-selected redshift and peculiar velocity survey that is complete to total extrapolated magnitude limits $(K_s, H, J) = (12.65, 12.95, 13.75)$ over 83% of the southern sky,

containing 125,071 redshifts in total; of these, 87,337 sources are extragalactic, have adequate redshift quality and are present in the ‘2MASS good’ sample, with $z_{\text{hel}} > 0$;

- 2dF Galaxy Redshift Survey (2dFGRS, Colless et al. 2001, 2003), with 226,906 galaxies of good-quality redshifts in an area of approximately 1500 deg² selected from the extended APM Galaxy Survey in three regions: a North Galactic Pole strip, a South Galactic Pole strip and random fields scattered around the SGP strip; of these, 46,150 are present in the ‘2MASS good’ sample within a matching radius of 3’’;
- The ZCAT compilation⁴, based on the CfA Redshift Catalog (Huchra et al. 1996), updated throughout the years by the late John Huchra. It contains 41,508 positive heliocentric redshift from the whole sky, of which only 9,267 matched 2MASS-good sources within 3’’ (this low matching rate might be due to inaccurate astrometry in the ZCAT).

These spectroscopic redshift surveys have some overlap, so that after adjusting for redundancy in total we obtained 464,857 positive heliocentric redshifts for the ‘2MASS good’ sample, which makes 32% of the total. In rare cases where conflicts in redshifts for the same object occurred, the priority was 2MRS > SDSS > 6dF > 2dF > ZCAT. The median redshift of the ‘2MASS-good-spectro’ sample is $z_{\text{med}} = 0.082$.

In Figure 4 we plot number counts as a function of the K_s -band magnitude for the 2MASS-good sources that have spectroscopic redshifts measured and for those that do not. This plot clearly shows that the spectroscopic data are not uniformly selected: the three ‘bumps’ in the magnitude distribution of spectro- z sources reflect the fact that the sample was compiled mainly from 2MRS, 6dFGS and SDSS. On the other hand, one can see that the spectroscopic redshifts are lacking only for objects with $K_s \gtrsim 11.5$, thanks to the all-sky completeness of the 2MRS below these magnitudes. The fact that number counts in the magnitude slice $11.75 < K_s < 12.85$ are

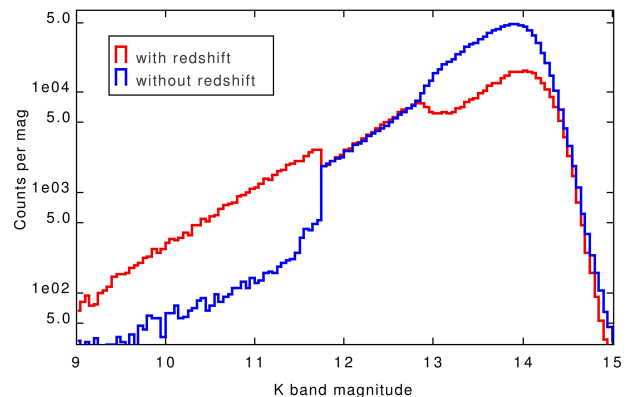


Figure 4. Number counts as a function of the K_s band magnitude for those 2MASS XSC sources that have spectroscopic redshift measurements (red line, 32% of the total sample) and for those that do not (blue line).

⁴ <https://www.cfa.harvard.edu/~dfabricant/huchra/zcat/>

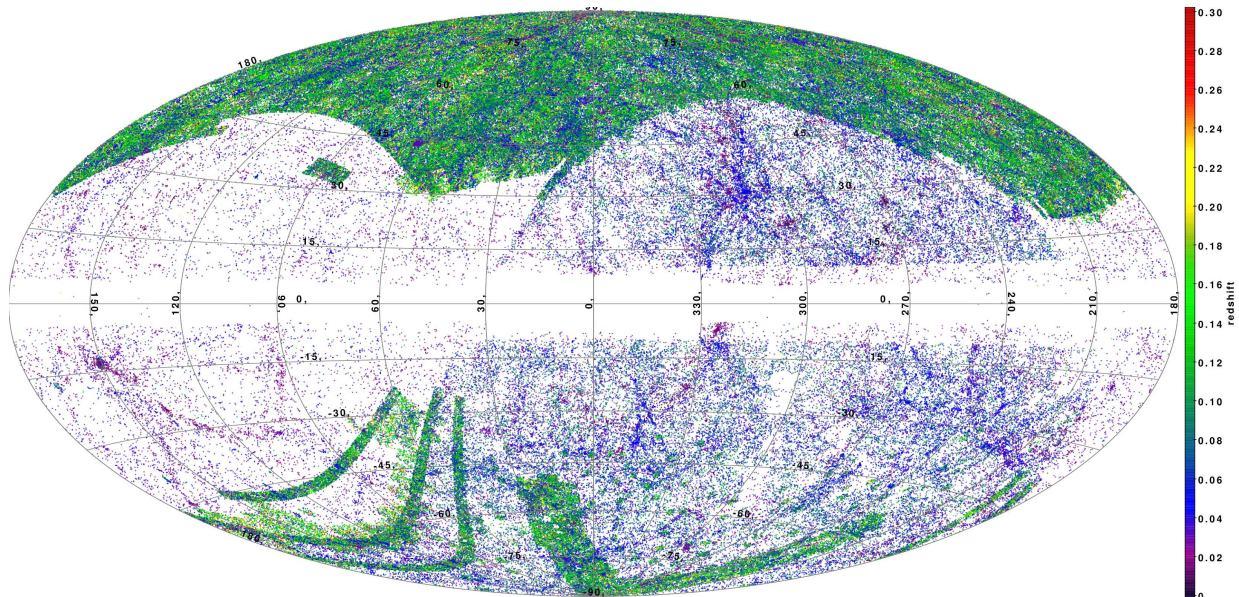


Figure 5.

Aitoff projection, in Galactic coordinates, of the all-sky source distribution of the 2MASS-good galaxies for which spectroscopic redshifts are presently available, as described in the text. This plot shows almost 465,000 sources.

very similar for sources with and without spectroscopy is just a coincidence: approximately half of the 2MASS galaxies at these magnitudes have redshifts from 6dFGS and SDSS, while the other half is located in the north not covered by SDSS and in the ZoA.

Figure 5 shows the Aitoff Galactic projection of all-sky distribution of the 2MASS-good sources with spectroscopic redshifts, color-coded by z_{spec} . This plot illustrates the fact that redshift completeness occurs only in the areas sampled by SDSS. If an all-sky *spectroscopic* redshift coverage of a depth comparable to 2MASS is ever to be obtained, a Southern analog of SDSS is essential, and the remaining gaps in the North need to be filled in. As things stand, the hope for progress towards this goal in the relatively near future relies on the success of the currently proposed TAIPAN survey (Colless et al. 2013). What can be additionally seen from Fig. 5 is that the large redshift surveys have been systematically avoiding the ZoA. Only the shallow 2MRS has probed into $|b| < 10^\circ$, still excluding the Galactic equator and bulge areas. This means that we practically do not have calibration data for photometric redshifts at low Galactic latitudes: only $\sim 3\%$ of all the 2MASS sources in this strip have spectroscopic information. However, we are still able to calculate photo- z 's within the ZoA by training on other parts of the sky. Nevertheless, due to problematic photometry (caused by stellar crowding and overestimated extinction correction), the photometric redshifts in this area are often underestimated.

In view of deriving photometric redshifts for the entire 2MASS catalog, an important caveat is whether this combined spectroscopic redshift sample is representative of the whole underlying dataset. This is not to say that equal sampling at all redshifts is required, but the full range of redshifts must be spanned, and examples of all the galaxy types at a given redshift are required. The actual 2MASS redshift distribution is of course not known, but certainly some of the above-listed redshift surveys will inevitably be shallower than an unbiased subsample

of the full survey. Among the redshift datasets we use, the closest to the actual 2MASS redshift distribution will be the SDSS DR9 in the main (contiguous) area in the North. As we discuss in Subsection 6.1, the majority (87%) of all 2MASS galaxies located in this region have redshifts measured from that survey. In our future cosmological applications of the photometric redshift catalog presented here we will have to make a trade-off between representativeness of the spectroscopic redshift sample used for photo- z estimation and its size. Note that there are, however, photometric redshift methods that, at least in principle, are independent of and do not require the usage of any training sets, such as for instance the EAZY package (Brammer et al. 2008).

In addition to the large-area redshift surveys listed above, which give the basis for the all-sky 2MASS photometric redshift estimation, we additionally used the recent data from the GAMA Data Release 2 (DR2; Liske et al. 2013, in prep.) to investigate the possibility of going deeper than with 2MASS XSC, while retaining all-sky coverage. This GAMA data release provides AAT/AAOmega spectra, redshifts and a wealth of ancillary information for 72,225 objects from the first phase of the GAMA survey (2008 – 2010, usually referred to as GAMA I). The GAMA I survey extends over three equatorial survey regions of 48 deg^2 each, called G09, G12 and G15 (Baldry et al. 2010). In DR2, data for all GAMA I main survey objects with $r < 19.0$ (G09 and G12) or $r < 19.4$ (G15) were released. We used the 70,330 DR2 sources with positive redshifts of quality $NQ > 2$. The median redshift of this sample is $z = 0.171$. Although it covers just a small fraction of the sky, its depth and completeness – better than that of the SDSS main galaxy sample – make GAMA an ideal catalog for all-sky photometric redshift calibration at larger distances than possible with 2MASS.

5. PHOTOMETRIC REDSHIFT FRAMEWORK

Methods for estimating photometric redshifts are now abundant, and fall under two general categories (and

combinations thereof): machine learning and spectral energy distribution (SED), or template, fitting. The first approach, proposed originally by Connolly et al. (1995), derives an empirical relation between magnitudes (and/or possibly other galaxy parameters, such as colors) and redshifts using a subsample of objects with measured spectroscopic redshifts, i.e. the *training set*. The trained algorithm (often additionally validated on a separate *validation set*) is then applied to the rest of the sample for which no spectroscopic redshifts are known. Machine learning methods generally rely on the availability of a sufficiently large and representative training set in order to be efficient and unbiased. However, they often do not require many photometric bands to perform successfully and even adding noisy measurements usually improves their performance.

The second general approach, the SED fitting procedure (e.g. Bolzonella et al. 2000), bases its efficiency on the fit of the overall shape of spectra and on the detection of strong spectral features. The observed photometric SEDs are compared to those obtained from a set of reference spectra, using the same photometric system. The photometric redshift of a given object corresponds to the best fit of its photometric SED by the set of template spectra. This method may be advantageous over machine learning as it usually does not require training sets. On the other hand, it needs accurate photometry – especially matching of seeing and apertures between passbands – and some prior knowledge of expected redshift distribution to perform efficiently.

As observed by Francis & Peacock (2010), photometric redshift estimation methods usually yield z_{phot} that are unbiased in a sense that the mean true redshift at given z_{phot} is equal to z_{phot} . But in order for this to be true, there must then be a bias in z_{phot} at given true z_{spec} , unless redshift distribution is constant. Since $N(z)$ in practice has a well-defined maximum, this means that z_{phot} will be overestimated near $z = 0$ and underestimated at high z .

Some of the particular implementations of the methods listed above have been compared in Abdalla et al. (2011), who applied them to ~ 1.5 million luminous red galaxies in SDSS DR6. Partially motivated by their results and by the fact that a significant fraction of our dataset already has spectroscopic redshifts measured, we employ the machine-learning approach. We have also made some early attempts into extending our study to SED-fitting methods, by testing the EAZY package (Brammer et al. 2008) on our data. Preliminary results are however not competitive with those described below, with accuracies typically 50% worse than in the machine-learning case. We suspect that this would arise also for other template-matching methods if used with our samples. The synthetic photometry may not match the real one for various reasons: the template spectra could be in error; we do not know the filter transmission curves perfectly (including the wavelength-dependent photographic sensitivity and the contribution of atmospheric absorption); aperture corrections may be slightly different in different bands if the seeing is wavelength-dependent. ANN z by its nature of using training sets from the data itself effectively self-calibrates and mitigates such systematics.

The need for SED templates was avoided by Francis & Peacock (2010), who took a highly direct approach to

the generation of photometric redshifts, averaging over neighbors of known redshift at a given location in the five-band magnitude space. By using magnitudes rather than colors, this automatically built in information from the luminosity function, so that bright galaxies were never allocated an extreme redshift that would require them to have an unrealistic luminosity. As a result, the scatter in photometric redshift declined towards $z = 0$. The overall rms in $z_{\text{phot}} - z_{\text{spec}}$ in the Francis & Peacock (2010) analysis was 0.033. This method is however limited by the need to bin the data, which requires an extremely large training set.

A non-exhaustive list of alternative photometric redshift estimators that use training sets includes such methods as Artificial Neural Networks (ANN, Firth et al. 2003; Tagliaferri et al. 2003; Collister & Lahav 2004; Vanzella et al. 2004; Way et al. 2009; Cavuoti et al. 2012), Support Vector Machines (Wadadekar 2005), Virtual Sensors (Way & Srivastava 2006), Random Forests (Carliles et al. 2010), Boosted Decision Trees (Gerdes et al. 2010), Weak Gated Experts (Laurino et al. 2011) or Self-Organized Maps (Geach 2012; Way & Klose 2012). Throughout our analysis, we applied a particular implementation of the first of these, namely the ANN z (Collister & Lahav 2004), leaving a possible comparison of different algorithm performance in our particular application for future work.

The ANN z package is freely available, ready-to-use software⁵ for photometric redshift estimation using artificial neural networks. For a detailed description of the ANN z algorithm and underlying methods, see Collister & Lahav (2004) and references therein. In short, it learns the relation between photometry and redshifts from appropriate training sets of galaxies for which the spectroscopic redshifts are already known. Whenever a sufficiently large and representative training set is available, ANN z is a highly competitive tool when compared with traditional template-fitting methods (Firth et al. 2003; Collister & Lahav 2004; Wang et al. 2009; Abdalla et al. 2011) and has been used for various data sets, including SDSS (Collister et al. 2007), GAMA (Christodoulou et al. 2012) or the Blanco Cosmology Survey (Desai et al. 2012). As we show in the remaining analysis, also in our application the ANN z does a very commendable job as gauged in both systematic and random errors.

6. PHOTOMETRIC REDSHIFT RESULTS: TEST FIELDS FOR 2MASS AND BEYOND

Before constructing the 2MASS Photometric Redshift catalog, which will be described in Section 7, we selected three test fields to verify how photometric redshift estimation performs for 2MASS-based data. We aimed at choosing such areas on the sky that would contain a sufficiently high number of galaxies each to clearly demonstrate the potential of the machine-learning methods for all-sky photometric redshift estimation. Additionally, these fields were defined in a way to emphasize possible biases and caveats, such as non-representativeness of the underlying spectroscopic redshift sample for the whole photometric set or the proximity of the Galactic Plane (ZoA) and resulting high extinction or stellar contamination. Finally, separate treatment of the GAMA

⁵ <http://www.homepages.ucl.ac.uk/~ucapola/annz.html>

fields served as a test-bed for our future work that will be based on WISE instead of 2MASS XSC data. The test fields discussed below are:

- North Galactic Cap (NGCap), defined as a circular region with $b_{\text{Gal}} > 60^\circ$;
- South Galactic Cap (SGCap), a circular region with $b_{\text{Gal}} < -60^\circ$;
- North Ecliptic Cap, a circular region for which $b_{\text{ecliptic}} > 60^\circ$;
- GAMA equatorial regions, composed of 3 rectangles enclosed within the following equatorial coordinates: (G09) $129^\circ \leq \alpha \leq 141^\circ$ and $-1^\circ \leq \delta \leq 3^\circ$; (G12) $174^\circ \leq \alpha \leq 186^\circ$ and $-2^\circ \leq \delta \leq 2^\circ$; (G15) $211^\circ \leq \alpha \leq 224^\circ$ and $-2^\circ \leq \delta \leq 2^\circ$.

As the purpose of the present Section is to verify the performance of ANNz in view of creating all-sky photometric redshift samples, the ‘spectroscopic-only’ sample for each field was further divided (randomly) into disjoint training, validation and test sets, respectively proportioned as 5:1:12. The proportion 1:2 between the calibration (training+validation) and test samples was chosen to mimic the actual situation with the 2MASS data, where every third galaxy has the spectroscopic redshift measured. Relative sizes of the training and validation sets were chosen somewhat arbitrarily, which however has no significant influence on the results, as long as both are sufficiently large, which is always the case here. The test sets were not used in the photo- z calibration procedure and served only for comparison purposes.

In addition to the preliminary selections applied to 2MASS, WISE and SCOS data described in Section 4, we additionally cleaned the samples used for the photometric redshift calibration by removing the sources fulfilling any of the following conditions: $z_{\text{spec}} \leq 0.003$ and high-redshift outliers; errors in any of the magnitudes $\Delta(\text{mag}) \geq 0.2$; relative errors in z_{spec} (when available) larger than 10%; reddening $E(B - V) \geq 0.25$. This filtering removed however only a small fraction of the spectroscopic samples.

The optimal architectures of the neural networks depended on the field and varied with number of inputs and size of training sets, but usually two intermediate layers with 6 to 23 nodes each sufficed. Committees of 6 to 30 networks, each trained with a different initial seed, were used. The inputs for the ANNz were the magnitudes in the photometric bands used, i.e. J, H, K_s from 2MASS, $W1, W2$ from WISE and B, R, I from SCOS, supplemented with WISE differential photometry $w1\text{mag}_1 - w1\text{mag}_3$ as an additional parameter whenever WISE data were used. The latter input allowed to automatically correct WISE profile-fit photometry for extended emission, see the discussion in Sec. 4.2. We checked that employing for instance a 2MASS angular size in addition to the WISE differential aperture magnitude gives tiny gain in photo- z accuracy, while every new parameter for the training considerably inflates computation time, especially for the full-sky sample.

We have also verified whether additional input parameters, uncorrelated with the spectroscopic redshift, could help mitigate some possible systematics. The latter were

identified by a posteriori checks of the photometric redshift samples; in particular, at low Galactic latitudes, wherever both extinction is severe and local star density is high, a small fraction of photo- z ’s are significantly underestimated. Looking for possible remedies, we considered the following inputs for the ANNz: Galactic extinction, angular coordinates and local star density⁶. None of them helped remove the bias nor improve overall statistics. The reason is that the photometry of the discussed sources is systematically compromised: first, the Schlegel et al. (1998) maps are known to overestimate extinction corrections at low Galactic latitudes; second, galaxy fluxes are polluted by Milky Way stars often superimposed on galaxy images. Both these effects cause the problematic sources to be seen as bluer and brighter than they actually are. This results in their photometric redshifts being systematically too low, which cannot be overcome by ‘regularizing’ ANNz performance with additional input parameters.

Each test field, as well as the all-sky sample, was treated separately, in a sense that the neural networks were optimized to each specific case by being trained independently. In addition, as discussed in Subsec. 4.3, separate networks were trained for the sources above and below $\delta_{1950} = 2.5^\circ$.

In order to quantify how ANNz performs, we calculate and report the following statistics for the test samples in each of the regions:

- mean $\langle z \rangle$ and median \bar{z} redshift of the true z_{spec} (input) and the calculated z_{phot} (output) distribution;
- 1σ scatter⁷ between the spectroscopic and photometric redshifts, $\sigma_{\delta z} = \langle (z_{\text{phot}} - z_{\text{spec}})^2 \rangle^{1/2}$;
- scaled median absolute deviation, defined as $\text{SMAD}(\delta z) = 1.4826 \times \text{med}(|\delta z - \text{med}(\delta z)|)$, a more robust measure of statistical dispersion, less prone to outliers than $\sigma_{\delta z}$;
- net bias of z_{phot} : $\langle \delta z \rangle = \langle z_{\text{phot}} - z_{\text{spec}} \rangle$;
- median of the relative error, where the latter is defined as $\Delta z = |z_{\text{phot}} - z_{\text{spec}}| / z_{\text{spec}}$ (expressed in per cent);
- percentage of outliers for which $|z_{\text{phot}} - z_{\text{spec}}| > 3 \text{SMAD}(\delta z)$.

Note that we have chosen to use the term ‘outliers’, without identifying them as ‘catastrophic’, as the latter are ambiguously defined in the literature (see e.g. Ilbert et al. 2006; Brammer et al. 2008; Oyaizu et al. 2008; Brescia et al. 2013 for different variants). If we chose to count the sources with $|z_{\text{phot}} - z_{\text{spec}}| > 3\sigma_{\delta z}$ instead of those outside $3 \text{SMAD}(\delta z)$, as in Oyaizu et al. (2008) and Gerdes et al. (2010), the numbers quoted below would decrease 2–3 times to typically 1%.

For the first three fields (the Caps), we present results of the photo- z estimation based on from 5 to 8 bands in total plus one WISE differential photometry parameter

⁶ 2MASS coadd $\log(\text{density})$ of stars with $K < 14$.

⁷ Note that we do *not* remove outliers in δz prior to calculating this statistic, so it may overestimate the actual scatter.

where relevant. Including WISE and especially SCOS in addition to 2MASS greatly improves the statistics of the $z_{\text{spec}} - z_{\text{ANN}z}$ comparison. On the other hand, adding SCOS slightly lowers the matching rate since not all the 2MASS×WISE sources are also present in SCOS with reliable photometry.

For the GAMA regions, however, we experiment with matching only WISE with SCOS, thus attempting measurements at greater depths (further described below, Subsection 6.4). This exploratory work gives a first taste of what will be possible when WISE is matched with higher-fidelity samples such as Pan-STARRS (Kaiser et al. 2002), SkyMapper (Keller et al. 2007) or VISTA-VHS (McMahon 2012).

6.1. North Galactic Cap

This region of $\sim 2800 \text{ deg}^2$ contains 131,707 ‘2MASS-good’ sources. Of these, over 99% have matches with the ‘WISE clean’ sample within a $3''$ radius and more than 97% of the total were identified in the SCOS as having all three *BRI* extended-source magnitudes measured. The combined 2M×WI×SC data set includes more than 127k of the original 2MASS XSC sources.

Our NGCap is an area fully covered by the SDSS main (contiguous) region and the majority of the 2MASS objects (87%) have spectroscopic redshifts measured from this survey, plus some from other catalogs. Note however that in the eventual all-sky applications these samples will be smaller, as the 2MASS catalog needs to be flux-limited at $K_s \lesssim 14$ to preserve its uniform depth on the sky (the full dataset is deeper in the North, for $\delta \gtrsim 12^\circ$). Here, we do *not* apply any flux limit as it has no important influence on our tests other than lowering the number of sources used for the photo- z estimation.

Having applied all the selection on the data, for the 2M×WI×SC sample we were left with fewer than 31k NGCap sources for neural network training and about 74.5k objects in the test set, and slightly larger respective sets for the 2M×WI and 2M×SC matches. The statistics for the ANN z application are summarized in Table 1. We can note that: (a) already the 2MASS×WISE sample allows for a photo- z accuracy comparable to that achieved by Francis & Peacock (2010) from 2MASS×SCOS matching (using only *B* and *R* bands); (b) the 2MASS×SCOS(*BRI*) option gives better results, at a cost of a slightly lower matching rate; and (c) combining the three surveys together greatly improves the photo- z estimates, which makes it the optimal approach. In particular, here as well as in the other test fields, supplementing 2MASS×WISE with the three SCOS bands ameliorates overall photometric redshift precision by 30% or better.

The results are visualized in the density plot (Figure 6(a)), which compares spectroscopic and photometric redshifts for the NGCap region. Since our photo- z estimation uses magnitudes and not colors, the same effects as discussed in Francis & Peacock (2010) are observed. The scatter in photometric redshifts declines towards $z = 0$ and the mean true (spectroscopic) redshift at a given z_{phot} is equal to z_{phot} ; but the photometric redshifts are overestimated near $z = 0$ and underestimated at high z . This is illustrated in Figs. 7(a) and 7(b) and applies equally to all the datasets discussed below.

A comparison of input spectroscopic and output pho-

tometric redshift distributions for the same test set, in the case where 8 bands were used, is shown in Figure 8. The shape of $N(z)$ is preserved to good accuracy over most of the redshift range. This is especially useful in applications where proper distributions in different redshift slices are needed, rather than the knowledge of individual galaxy redshifts, and will be taken advantage of in the forthcoming ISW analysis using this catalog together with Planck data (Steward et al., in prep.).

6.2. South Galactic Cap

This region has the same area as the NGCap, but it is considerably different in terms of the spectroscopic redshifts available: out of almost 113,000 ‘2MASS-good’ sources in the region, 36% have redshifts, the bulk of which come from the 2dFGRS, 6dFGS and SDSS (southern strips). Moreover, the median redshift of the spectroscopic sample is here considerably smaller than in the NGCap. This difference does not reflect the actual redshift distribution of 2MASS galaxies; on the contrary, the North includes Virgo and Coma clusters, whereas no such nearby overdensities exist in the SGCap.

As in the other fields, the matching rate of 2MASS-good with WISE-clean is over 99%, it amounts to over 97% for 2MASS×SCOS and is slightly below 97% for 2M×WI×SC combined. Having applied all the cuts on the data, in the 8-band case we were left with over 10.8k spectroscopic redshifts for neural network training and 26.2k objects in the test set, and respectively larger numbers for the 2M×WI and 2M×SC matches. The results of applying the ANN z are again summarized in Table 1. The statistics here are comparable to the NGCap case, despite the much smaller spectroscopic sample. Figure 6(b) shows a density plot comparing spectro- and photo- z ’s when all the 8 bands are used.

6.3. North Ecliptic Cap

This field is located closer to the Galactic Plane: approximate Galactic coordinates of the of the North Ecliptic Pole are $\ell_{\text{NEP}} = 96.4^\circ$, $b_{\text{NEP}} = 29.8^\circ$. There are several reasons for choosing such a test field. First, it stretches out to the Zone of Avoidance of low Galactic latitudes, where the density of 2MASS XSC sources decreases considerably and the Galactic extinction becomes significant, even at infrared wavelengths. On the other hand, due to the WISE surveying strategy, its depth is much higher in the ecliptic caps than in the rest of the sky, reaching 5σ depths of $30 \mu\text{Jy}$ for *W1* (Jarrett et al. 2011). Finally, SCOS becomes less reliable near the ZoA due to high extinction and to blends of point sources (i.e., stars) that mimic extended ones. In view of future all-sky applications, our goal was to verify the influence of these effects on the photo- z estimates.

There are fewer than 98,000 ‘2MASS-good’ sources in the region, considerably fewer than in the Galactic Caps of the same area, and their number density decreases near the Galactic plane due to lower sensitivity in the 2MASS extended source catalog, arising from stellar confusion (Jarrett 2004). Of these, $\sim 97\%$ sources have matches with ‘WISE-clean’ sample within a matching radius of $3''$, and the matching rate decreases towards lower Galactic latitudes, emphasizing the deleterious influence of stellar confusion noise. Also the percentage of matches

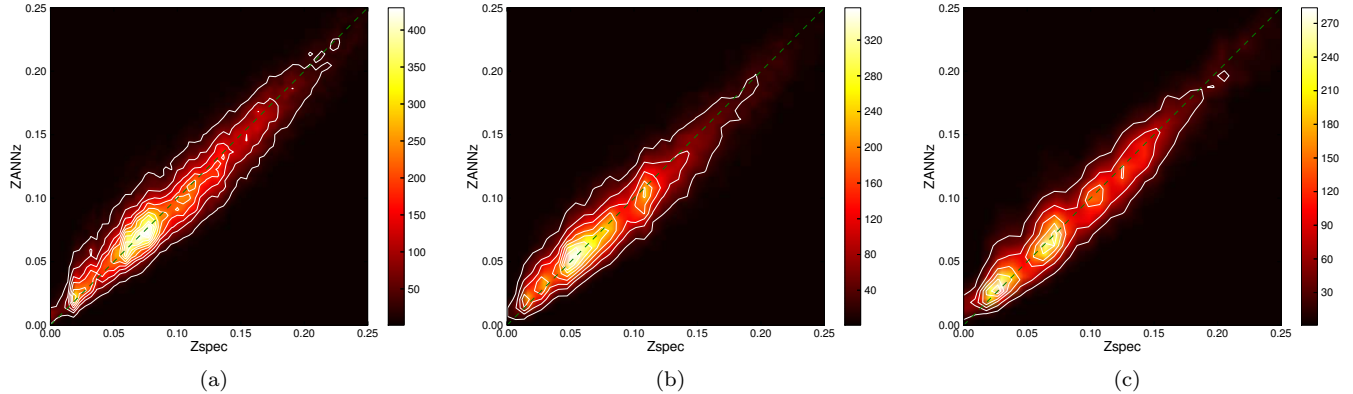


Figure 6. Comparison of spectroscopic and photometric redshifts for 2MASS×WISE×SCOS matches (8 photometric bands) in: (a) the North Galactic Cap, $b_{\text{Gal}} > 60^\circ$ (over 74,000 sources in the test set); (b) the South Galactic Cap, $b_{\text{Gal}} < -60^\circ$ (over 26,000 sources in the test set); the North Ecliptic Cap, $b_{\text{ecl}} > 60^\circ$ (roughly 9,000 sources in the test set).

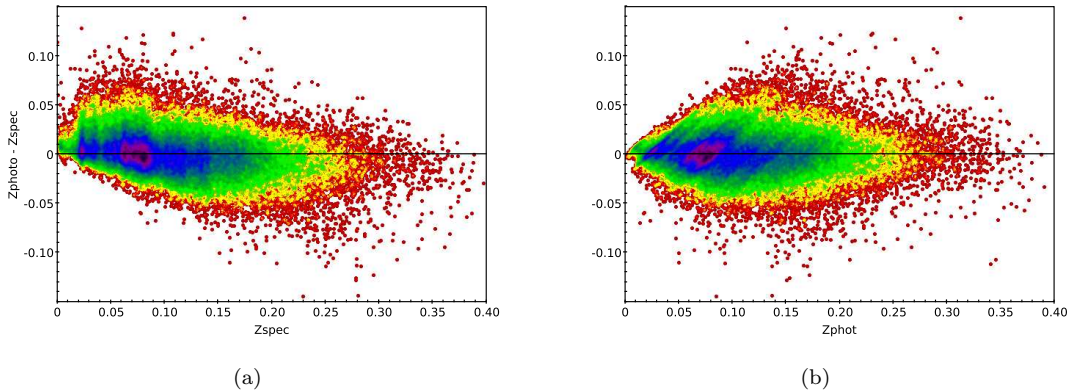


Figure 7. Error in the photo- z as a function of (a) spectroscopic redshift and (b) photometric redshift. These plots illustrate the general property of the photo- z 's being unbiased in a sense that the mean true redshift at given z_{phot} is equal to z_{phot} , while they are overestimated near $z_{\text{spec}} = 0$ and underestimated at high z .

of 2MASS XSC with SCOS sources is lower than in the two other test fields, amounting here to 95%. The resulting 8-band 2M×WI×SC sample includes almost 91,000 sources.

The redshift coverage is relatively poor: about 20,000 galaxies have spectroscopy in this region, mainly from the SDSS and 2MRS. After all the relevant cuts, the training and test sets contained respectively $\sim 5,500$ and $\sim 13,000$ sources. We note that in the training and vali-

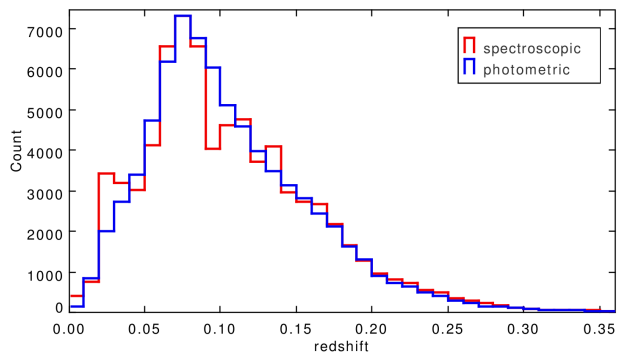


Figure 8. Comparison of redshift distributions for the test set in the North Galactic Cap: original spectroscopic sample in red and resulting photometric redshifts in blue, where 8 bands from 2MASS×WISE×SCOS were used.

ation sets, most of the sources near the Galactic Plane were removed due to the high extinction level (for training we use only those with $EBV < 0.25$, equivalent to a B -band extinction of ~ 1 mag). Nevertheless, the performance of the ANN z redshift estimation – tested on a sample disjoint with the training set, but where all the available sources with spectroscopic redshift, also those from high EBV regions, were retained – is here similar to the two previous cases and is summarized in Table 1. Again the additional three SCOS bands give the best improvement for the photo- z 's over 2MASS×WISE only. Figure 6(c) shows the relevant density plot for spectroscopic and photometric redshift comparison.

6.4. Advancing beyond 2MASS: GAMA regions

In this Subsection we move beyond the use of 2MASS as a basic dataset for photometric redshift estimation, with the eventual aim of reaching significantly larger depths over the entire sky. We selected well-studied equatorial fields as a test-bed for future applications relying mainly on WISE data. Since both the WISE and SCOS catalogs are considerably deeper than 2MASS XSC, we matched the two former in these areas and used the currently available GAMA DR2 spectroscopic data (Liske et al. 2013, in prep.) to test the performance of the ANN z in these fields, in view of a future all-sky WISE×SCOS

Table 1
Statistics for the photometric redshift estimation for the 2MASS-based test samples.

cross-matched surveys ^a	number of sources ^b	mean $\langle z \rangle$ spec ^c	mean $\langle z \rangle$ phot ^d	median \bar{z} spec ^c	median \bar{z} phot ^d	1σ scatter ^e $\sigma_{\delta z}$	scaled MAD ^f	net bias ^g $\langle \delta z \rangle$	median error ^h	% of outliers ⁱ
North Galactic Cap										
2MASS×WISE	75,754	0.106	0.105	0.095	0.099	0.031	0.024	-3.6e-5	17.1%	3.2%
2MASS×SCOS	74,866	0.106	0.106	0.095	0.097	0.025	0.022	4.7e-6	15.0%	1.6%
2M×WI×SC	74,538	0.106	0.106	0.095	0.095	0.019	0.016	-6.0e-5	11.2%	2.4%
South Galactic Cap										
2MASS×WISE	26,692	0.092	0.092	0.082	0.085	0.027	0.021	1.2e-4	17.1%	3.7%
2MASS×SCOS	26,353	0.093	0.093	0.082	0.085	0.023	0.019	2.1e-6	15.8%	2.3%
2M×WI×SC	26,208	0.093	0.093	0.083	0.083	0.019	0.015	-7.5e-5	12.1%	3.0%
North Ecliptic Cap										
2MASS×WISE	13,104	0.098	0.097	0.086	0.092	0.030	0.022	-7.0e-4	17.4%	3.7%
2MASS×SCOS	12,932	0.099	0.098	0.087	0.092	0.024	0.020	-6.9e-4	15.9%	2.4%
2M×WI×SC	12,844	0.099	0.099	0.087	0.089	0.019	0.015	-5.4e-5	11.5%	2.8%
All-sky spectroscopic sample										
2MASS×WISE×SCOS										
no flux limit	300,986	0.094	0.094	0.083	0.084	0.019	0.015	-1.5e-5	12.1%	3.0%
$K_s < 13.9$ mag	207,151	0.078	0.078	0.070	0.070	0.017	0.013	-4.9e-5	12.9%	2.9%

^a 2M = 2MASS XSC (3 bands J, H, K_s); WI = WISE (2 bands $W1, W2$ + differential photometry); SC = SuperCOSMOS (3 bands B, R, I).

^b In the test set.

^c Input (spectroscopic) redshift sample.

^d Output (photometric) redshift sample.

^e 1σ scatter between the spectroscopic and photometric redshifts, $\sigma_{\delta z} = \langle (z_{phot} - z_{spec})^2 \rangle^{1/2}$.

^f Scaled median absolute deviation, $SMAD(\delta z) = 1.48 \times \text{med}(|\delta z - \text{med}(\delta z)|)$.

^g Net bias of z_{phot} : $\langle \delta z \rangle = \langle z_{phot} - z_{spec} \rangle$.

^h Median of the relative error.

ⁱ Percentage of outliers for which $|z_{phot} - z_{spec}| > 3 SMAD(\delta z)$.

photo- z sample. In total, we had almost 70,000 good-quality spectroscopic redshifts released so far within the GAMA project (with $z > 0.0015$ to avoid stellar contamination). As the total area of the GAMA fields that we used is 144 deg^2 , it is clear that the GAMA number density is much higher than that of the 2MASS XSC (less than 30 sources per deg^2), and indeed, only about 5000 of the GAMA galaxies are also present in the 2MASS-good sample. On the other hand, the ‘clean’ WISE data matched with the SCOS catalog within $2''$ give more than 227k pairs in the GAMA regions. Matching those additionally with the GAMA DR2 spectroscopic sources, also within $2''$, provides 63,000 ‘GA×WI×SC’ objects. These numbers apply to those SCOS sources that have B and R extended-source photometry in the catalog; the I band is shallower and if also used, the sample reduces to 60.2k objects. This analysis also confirms that both WISE and SCOS data are deeper than the current GAMA release and the redshift distribution of the cross-matched sample reflects the current depth of GAMA rather than of WISE×SCOS. As for the key numbers, there are over 380,000 B, R -selected SuperCOSMOS extended sources in the GAMA regions and over 1 million WISE objects with $w1snr \geq 5$ and $w2snr \geq 2$.

The overall sample has up to 5-band data for the photometric redshift estimation. As we show below, this is sufficient to obtain average photo- z accuracy similar to the 2MASS-based analyses described in this paper, when rescaled to higher redshifts. Appropriate filtering of the data and removal of redshift outliers gave us finally a

sample of almost 20,000 GA×WI×SC(BR) sources for network training and validation (and slightly fewer with the I band added). The results of applying the trained ANN z to the test sets are summarized in Table 2 and illustrated in Figure 9 comparing spectroscopic and photometric redshifts of the test sample.

It is significant that even with only 4 bands used we are achieving accuracies comparable to shallower 2MASS-based samples when 5 bands (2MASS×WISE) were applied. This is very promising for future WISE×SCOS

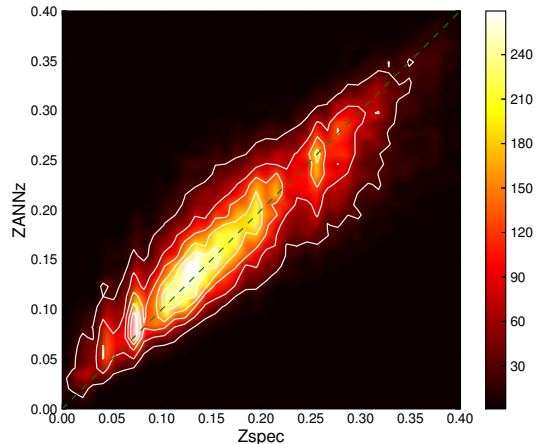


Figure 9. Comparison of spectroscopic and photometric redshifts for the GAMA regions (WISE×SCOS photometry, 4 bands; over 40,000 sources in the test set).

Table 2
Statistics for the photometric redshift estimation in the GAMA regions.

cross-matched surveys ^a	number of sources ^b	mean $\langle z \rangle$ spec ^c	mean $\langle z \rangle$ phot ^d	median \bar{z} spec ^c	median \bar{z} phot ^d	1σ scatter ^e $\sigma_{\delta z}$	normalized $\sigma_{\delta z}/(1+z)$	scaled MAD ^f	net bias ^g $\langle \delta z \rangle$	median error ^h	% of outliers ⁱ
GAMA regions											
WI×SC _{BR}	41,556	0.186	0.186	0.175	0.180	0.044	0.036	0.034	-2.7e-4	13.9%	3.3%
WI×SC _{BRI}	39,536	0.185	0.185	0.174	0.180	0.043	0.035	0.034	1.8e-4	13.7%	3.1%

^a WI = WISE (2 bands $W1, W2$); SC = SuperCOSMOS (2 or 3 bands B, R, I).

^b In the test set.

^c Input (spectroscopic) redshift sample.

^d Output (photometric) redshift sample.

^e 1σ scatter between the spectroscopic and photometric redshifts, $\sigma_{\delta z} = \langle (z_{\text{phot}} - z_{\text{spec}})^2 \rangle^{1/2}$.

^f Scaled median absolute deviation, $\text{SMAD}(\delta z) = 1.48 \times \text{med}(|\delta z - \text{med}(\delta z)|)$.

^g Net bias of z_{phot} : $\langle \delta z \rangle = \langle z_{\text{phot}} - z_{\text{spec}} \rangle$.

^h Median of the relative error.

ⁱ Percentage of outliers for which $|z_{\text{phot}} - z_{\text{spec}}| > 3 \text{SMAD}(\delta z)$.

and more generally WISE×optical all-sky photo- z samples, although it requires further investigation. Adding the 5th band (SCOS I) leads to only slight improvement and lowers the matching rate. Moreover, as the SCOS I -band data are reliable only to $I \lesssim 19$, in our future applications using the forthcoming full GAMA I spectroscopic dataset (which will be complete to $r \leq 19.4$) and especially the GAMA II depth of $r \leq 19.8$, this additional SCOS band will have to be discarded to preserve the completeness of the WISE×SCOS sample. Similarly, the WISE $W3$ and $W4$ bands may have too low detection rates at these depths to be applicable.

Having verified the performance of the ANN z on the test set, we trained the neural networks on all the GA×WI×SC cross-matches and applied them to the WISE objects in GAMA areas that paired up with an SCOS extended source. In Figure 10 we compare the input spectroscopic redshift distribution with the derived photometric redshifts for two flux-limited samples: one with $R < 19.5$ and the other with $R < 20.0$. These samples contain respectively 130k and 181k sources, and their median photometric redshifts are respectively 0.19 and 0.23 (compared to 0.17 in GAMA DR2). Normally it is safe to extrapolate ANN z results in this way to slightly greater depths than the calibrat-

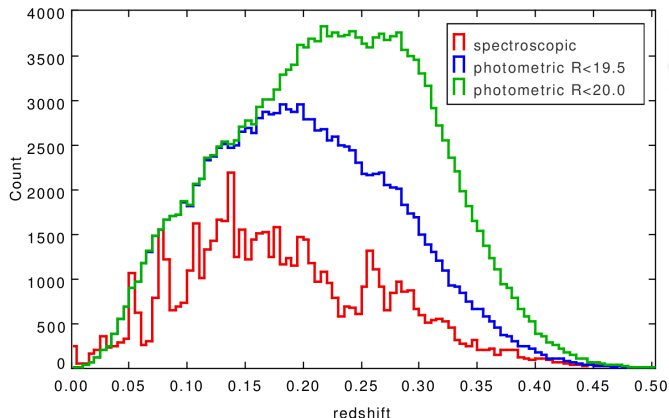


Figure 10. Redshift distribution of the spectroscopic GAMA DR2 sample (in red) and of the resulting photometric redshifts calculated for the WISE×SCOS cross-matches in GAMA areas: flux-limited at $R < 19.5$ in blue and at $R < 20.0$ in green.

ing spectroscopy. The full cross-matched WISE×SCOS sample reaches beyond $R = 20$, but to properly calibrate photometric redshifts at these depths we would need higher redshift coverage from future GAMA releases, as the present DR2 sample is limited to $r < 19.4$ in one of the fields and to $r < 19.0$ in the two other. Nevertheless, a clear conclusion is that cross-matching WISE with SuperCOSMOS gives the potential to obtain an all-sky sample reaching a median redshift of at least ~ 0.25 .

We note finally that other redshift surveys will be of additional use for the all-sky WISE-based photometric redshift estimation, such as for instance SDSS-III. The galaxy redshift sample in the most recent Data Release of SDSS, DR10 (Ahn et al. 2013), has a median redshift of already $z \simeq 0.3$, as it includes many higher- z sources thanks to the ongoing Baryon Oscillation Spectroscopic Survey (BOSS, Dawson et al. 2013) observations. Combining current and future releases of SDSS and GAMA with legacy samples such as the 2dFGRS should provide representative training sets for the all-sky WISE×SCOS dataset that is expected to reach up to 3 times deeper than the 2MASS-based sample presented below. One of the potential uses of this deep 3D catalog will be to select and refine sources to target for dedicated large-area multi-object spectroscopic surveys, notably the TAIPAN concept to cover the entire southern hemisphere to depths comparable to SDSS (Colless et al. 2013). Among the necessary conditions for this to be achieved are the availability of a WISE extended source catalog and proper star-galaxy separation for the unresolved WISE sources (Świątoń et al., in prep.).

7. THE TWO MICRON ALL-SKY PHOTOMETRIC REDSHIFT CATALOG

The tests performed in the three Caps, described above, prove that we have achieved the goal of reliable photometric redshift estimation for the entire 2MASS XSC, with controlled and impressively small errors, as well as a low percentage of outliers. As we have shown, when no flux limit is imposed on the sample, the (unclipped) 1σ scatter is below 0.02 at a median $z \sim 0.1$, scaled median absolute deviation is about 0.015 and the median of relative error in photometric redshifts amounts to $\sim 12\%$. Before generating the 2MASS Photometric Redshift catalog, we made the final checks by training

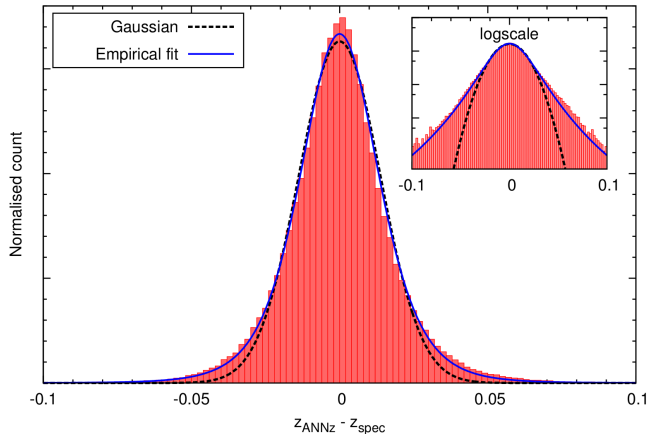


Figure 11. Error distribution between the photometric and spectroscopic redshifts for the 2MASS Photometric Redshift sample (red bars). The blue solid line is the empirical fit given by Eq. (4) with $a = 3.2$ and $s = 0.0125$; the black dashed line shows a best-fit Gaussian with $\sigma = 0.0138$.

and testing the neural networks on the *all-sky* spectroscopic sample, described in Subsec. 4.4. We proceeded in exactly the same way as discussed in Section 6, and the results are also given in Table 1 (‘All-sky spectroscopic sample’). We provide two sets of statistics: one for the full sample without any flux limit and another for sources with $K_s < 13.9$, the latter being the all-sky completeness limit of 2MASS XSC. These numbers confirm our findings from the test fields, showing that flux-limiting the sample has little influence on the accuracy.

In Figure 11 we plot the error distribution $\delta z \equiv z_{\text{phot}} - z_{\text{spec}}$ for the all-sky sample (red bars). Its shape is non-Gaussian in the wings and we prefer to use a more flexible fitting form instead. Namely, we chose to approximate it by

$$N(\delta z) \propto (1 + \delta z^2 / 2as^2)^{-a}, \quad (4)$$

with $a \simeq 3.2$. For such a distribution, 68% of the probability lies between $-1.2s$ and $+1.2s$ and thus defined ‘ 1σ ’ is constant at ~ 0.02 above $z = 0.1$, but is smaller at lower redshifts. For the whole sample, best-fit $s = 0.0125$, which is consistent with the average scatter of ~ 0.015 . On the other hand, a Gaussian gives a much worse approximation here. For a best-fit $\sigma = 0.0138$, the central part is reasonably well matched, however the wings are underestimated. This is especially pronounced in the logscale inset of Fig. 11. Note also that if analyzed in narrow redshift bins, then at the low- and high- z tail the distribution will no longer be centered on 0 nor even symmetric, which reflects the properties discussed already above and illustrated in Fig. 7(a).

Having checked the above properties of the photometric redshifts, we used the all-sky 2MASS×WISE×SCOS spectro- z sample as training and validation sets and applied thus trained neural networks to all the 2MASS galaxies from the ‘good’ sample, flux-limited at $K_s < 13.9$, matched with both WISE and SCOS. Out of one million 2MASS galaxies present in the complete sample, almost 94% were also identified in both the pre-filtered WISE $W1W2$ and SCOS BRI datasets, within a matching radius of $3''$.

The small fraction of the 2MASS XSC sources that do not have a counterpart in ‘clean’ WISE or/and SCOS,

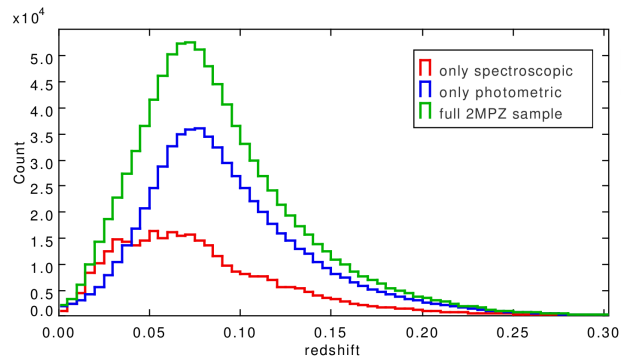


Figure 12. Comparison of redshift distributions in the all-sky 2MASS Photometric Redshift catalog: sources with spectroscopic redshifts in red, those with only photo- z ’s in blue and the full redshift sample in green.

are located mainly in the Galactic Plane and in the regions of high extinction and stellar confusion (30% of all the non-matches are within $|b| < 10^\circ$), as well as near the Magellanic Clouds and in the areas of WISE ‘torque rod gashes’ (cf. Figs. 2 and 3 and related discussion). Some of the unmatched galaxies are also randomly scattered over the entire sky (vicinity of bright stars, Galactic extended sources etc.), which slightly lowers the mean number density of the cross-matched sources with respect to the basic 2MASS XSC. The final 2MASS Photometric Redshift catalog (2MPZ), flux limited at $K_s < 13.9$, contains almost 935,000 galaxies with a mean redshift of $z = 0.08$, complete over 95% of the sky.

As already discussed, in the Galactic Plane ($|b| < 5^\circ$), where the Schlegel et al. (1998) extinction maps are known to be unreliable and stellar confusion is significant, the photometric redshifts are often biased low due to systematic errors in the photometry. In general, the regions of $|b| < 10^\circ$ are undersampled in our 2MPZ catalog, and especially so in the spectroscopic training sets. For these reasons the Galactic plane and the above-mentioned incompleteness areas should preferably be masked out for applications requiring all-sky uniformity. This still leaves more than 80% of the sky comprehensively and reliably mapped in 3 dimensions with our catalog, up to distances of ~ 500 Mpc.

Figure 12 compares the redshift distributions of the 2MPZ sample: input spectroscopic redshifts in red, derived photometric redshifts of the sources with no spectro- z measurements in blue, and the distribution of the full sample in green. Finally, Figure 13 shows the Aitoff projection, in Galactic coordinates, of the complete 2MPZ catalog, color-coded by z_{phot} . All the sources here have *photometric* redshifts shown, even those that already had spectroscopic ones measured. The cosmic web is clearly evident with filaments, clusters and voids, despite the tendency of photo- z ’s to dilute structures, as has been already illustrated by Jarrett (2004) where z_{phot} accuracy was considerably lower. Replacing photometric redshifts with spectroscopic ones (where available) hardly changes this overall picture.

8. SUMMARY AND FUTURE PROSPECTS

The main aim of this paper has been to show that by combining the largest all-sky galaxy catalogs it is possible to derive reliable and unbiased photometric redshifts over the entire sky, with reasonably small and controlled

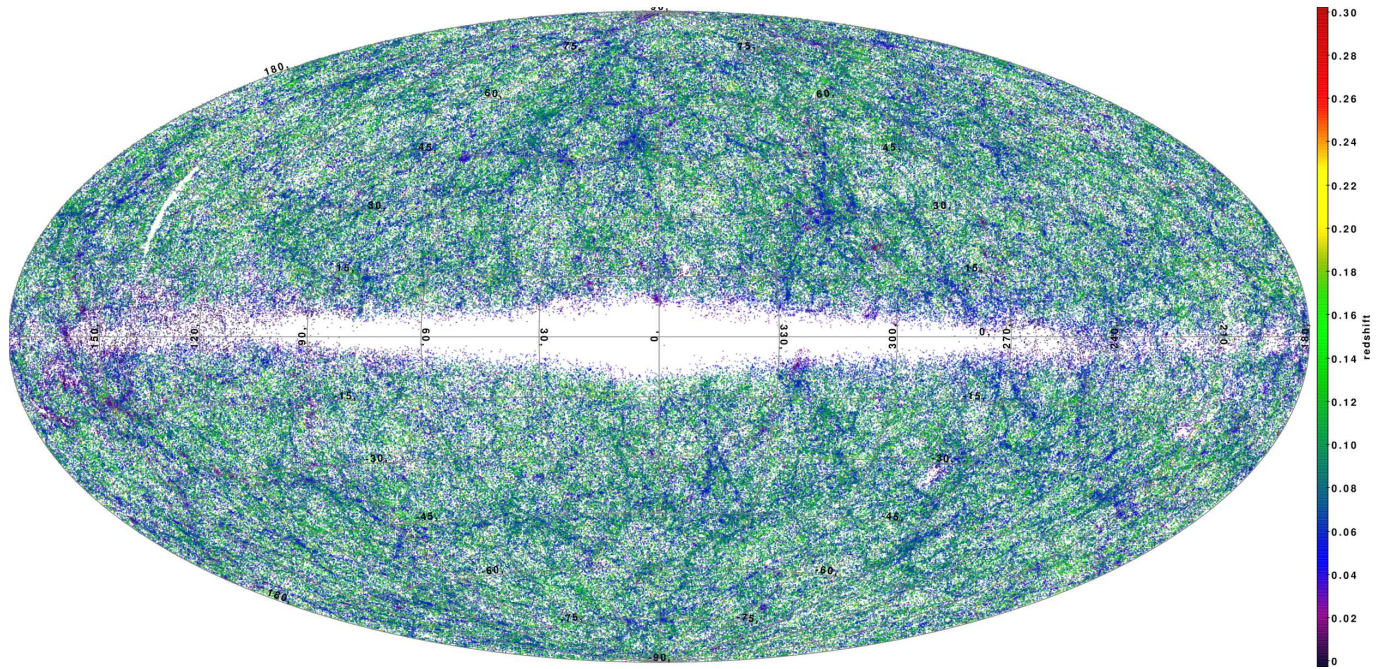


Figure 13.

Aitoff projection in Galactic coordinates of the all-sky source distribution in the 2MASS Photometric Redshift catalog, color-coded by photometric redshift. The cosmic web is evident despite the tendency of photo- z 's to dilute structures.

errors. We have focused mainly on the 2MASS XSC, and detailed tests on spectroscopic subsamples of this catalog have confirmed that we have met our goals. The resulting Two Micron All Sky Photometric Redshift catalog (2MPZ) contains 10^6 galaxies, of which 2/3 have redshifts estimated only photometrically using the 8 IR and optical bands of 2MASS, WISE and SuperCOSMOS, with a 1σ scatter of $\sigma_z = 0.015$, negligible mean bias and a very low fraction of outliers ($\sim 3\%$). Having a median $z \sim 0.1$, this is the largest all-sky redshift sample to date, and refines the earlier efforts of Jarrett (2004) and Francis & Peacock (2010), as well as expands the 2M++ catalog by Lavaux & Hudson (2011). Moreover, we have shown that it will be possible to obtain an all-sky 3D catalog of perhaps three times the 2MASS depth when WISE and SCOS are combined over the entire sky. For that purpose, we have used the latest redshift release of GAMA (DR2) as a test-bed, but there are many more redshift surveys available to train the photometric redshift algorithms on scales of $z \sim 0.25$. Obtaining such a WISE-based all-sky photometric redshift catalog will be our focus in the near future. This will also provide a pilot study for combining WISE with deeper large-area surveys that will be made available in the coming years, notably arising from Pan-STARRS and VISTA observations.

The applications of such three-dimensional datasets covering the whole sky will be manifold: more detailed analysis of the acceleration of the Local Group (the clustering dipole, e.g. Bilicki et al. 2011), of its convergence and sources of the pull (Kocevski & Ebeling 2006; Lavaux et al. 2010); bulk flow estimates on scales beyond the reach of peculiar velocities and independent of them, as well as of the kinetic Sunyaev-Zel'dovich measurements (Nusser et al. 2011; Branchini et al. 2012); measurement of the growth rate at low redshift, independent of redshift-space distortions or velocity field reconstructions

(Nusser et al. 2012); integrated Sachs-Wolfe effect (Francis & Peacock 2010) or other cross-correlations of the CMB with the LSS, such as gravitational lensing (Planck Collaboration et al. 2013a). The future WISE-based photometric redshift catalog will enable to extend to larger volumes such tests for large-scale structure isotropy as presented by Gibelyou & Huterer (2012).

In principle, our catalogs will be appropriate for any applications that require uniform all-sky photometry, precise knowledge of the redshift distribution of the sample, and of the angular, radial and photometric selection function. For most of the above applications, our precision of $\sigma_z \simeq 0.015$ will be adequate. In principle, this could be further improved by using surveys with an order of magnitude more photometric bands (e.g. J-PAS, Marín-Franch et al. 2012), although there are currently no plans for such surveys to cover the entire sky.

Acknowledgments.

We thank the Wide Field Astronomy Unit at the Institute for Astronomy, Edinburgh for archiving the 2MPZ catalog, which can be accessed at <http://surveys.roe.ac.uk/ssa/TWOMPZ>.

We thank the referee for useful comments improving the quality of this manuscript. We also benefited from discussions with Enzo Branchini, Adi Nusser and Ned Taylor. We are grateful to Nigel Hambly and Mike Read for providing SuperCOSMOS data in the north equatorial pole that were missing in the online database. Felipe Abdalla provided valuable help regarding the ANN z code.

Special thanks to Mark Taylor for his wonderful TOPCAT software, <http://www.starlink.ac.uk/topcat/> (Taylor 2005). Some of the results in this paper have been derived using the HEALPix package (Górski et al. 2005), <http://healpix.jpl.nasa.gov>.

This publication makes use of data products from the

Two Micron All Sky Survey⁸, Wide-field Infrared Survey Explorer⁹, SuperCOSMOS Science Archive¹⁰, Sloan Digital Sky Survey¹¹ and Galaxy And Mass Assembly¹² catalogs.

The financial assistance of the South African National Research Foundation (NRF) towards this research is hereby acknowledged. MB was partially supported by the Polish National Science Center under contract #UMO-2012/07/D/ST9/02785. MEC acknowledges support from the Australian Research Council (FS110200023).

REFERENCES

- Abdalla, F. B., Banerji, M., Lahav, O., & Rashkov, V. 2011, *MNRAS*, 417, 1891
- Afshordi, N., Loh, Y.-S., & Strauss, M. A. 2004, *Phys. Rev. D*, 69, 083524
- Ahn, C. P., et al. 2012, *ApJS*, 203, 21
- . 2013, *ArXiv e-prints*
- Baldry, I. K., et al. 2010, *MNRAS*, 404, 86
- Basilakos, S., & Plionis, M. 2006, *MNRAS*, 373, 1112
- Benítez, N. 2000, *ApJ*, 536, 571
- Beutler, F., et al. 2012, *MNRAS*, 423, 3430
- Bilicki, M. 2012, PhD thesis, Nicolaus Copernicus Astronomical Center, Polish Academy of Sciences
- Bilicki, M., Chodorowski, M., Jarrett, T., & Mamon, G. A. 2011, *ApJ*, 741, 31
- Bolzonella, M., Miralles, J.-M., & Pelló, R. 2000, *A&A*, 363, 476
- Brammer, G. B., van Dokkum, P. G., & Coppi, P. 2008, *ApJ*, 686, 1503
- Branchini, E., Davis, M., & Nusser, A. 2012, *MNRAS*, 424, 472
- Brescia, M., Cavuoti, S., D’Abrusco, R., Longo, G., & Mercurio, A. 2013, *ApJ*, 772, 140
- Cardelli, J. A., Clayton, G. C., & Mathis, J. S. 1989, *ApJ*, 345, 245
- Carliles, S., Budavári, T., Heinis, S., Priebe, C., & Szalay, A. S. 2010, *ApJ*, 712, 511
- Cavuoti, S., Brescia, M., Longo, G., & Mercurio, A. 2012, *A&A*, 546, A13
- Christodoulou, L., et al. 2012, *MNRAS*, 425, 1527
- Clarkson, C. 2012, *Comptes Rendus Physique*, 13, 682
- Colless, M., Beutler, F., & Blake, C. 2013, in *IAU Symposium*, Vol. 289, IAU Symposium, ed. R. de Grijs, 319–322
- Colless, M., et al. 2001, *MNRAS*, 328, 1039
- . 2003, *ArXiv Astrophysics e-prints*
- Collister, A., et al. 2007, *MNRAS*, 375, 68
- Collister, A. A., & Lahav, O. 2004, *PASP*, 116, 345
- Connolly, A. J., Csabai, I., Szalay, A. S., Koo, D. C., Kron, R. G., & Munn, J. A. 1995, *AJ*, 110, 2655
- Cutri, R. M., & et al. 2012, *VizieR Online Data Catalog*, 2311, 0
- Cutri, R. M., et al. 2012, *Explanatory Supplement to the WISE All-Sky Data Release Products*, Tech. rep.
- Davis, M., Nusser, A., Masters, K. L., Springob, C., Huchra, J. P., & Lemson, G. 2011, *MNRAS*, 413, 2906
- Dawson, K. S., et al. 2013, *AJ*, 145, 10
- Desai, S., et al. 2012, *ApJ*, 757, 83
- Driver, S. P., et al. 2009, *Astronomy and Geophysics*, 50, 050000
- Eisenstein, D. J., et al. 2011, *AJ*, 142, 72
- Erdogdu, P., et al. 2006, *MNRAS*, 368, 1515
- Firth, A. E., Lahav, O., & Somerville, R. S. 2003, *MNRAS*, 339, 1195
- Flaherty, K. M., Pipher, J. L., Megeath, S. T., Winston, E. M., Gutermuth, R. A., Muzerolle, J., Allen, L. E., & Fazio, G. G. 2007, *ApJ*, 663, 1069
- Francis, C. L., & Peacock, J. A. 2010, *MNRAS*, 406, 2
- Geach, J. E. 2012, *MNRAS*, 419, 2633
- Geach, J. E., et al. 2013, *ApJ*, 776, L41
- Gerdes, D. W., Sypniewski, A. J., McKay, T. A., Hao, J., Weis, M. R., Wechsler, R. H., & Busha, M. T. 2010, *ApJ*, 715, 823
- Gibelyou, C., & Huterer, D. 2012, *MNRAS*, 427, 1994
- Górski, K. M., Hivon, E., Banday, A. J., Wandelt, B. D., Hansen, F. K., Reinecke, M., & Bartelmann, M. 2005, *ApJ*, 622, 759
- Hambly, N. C., Davenhall, A. C., Irwin, M. J., & MacGillivray, H. T. 2001a, *MNRAS*, 326, 1315
- Hambly, N. C., Irwin, M. J., & MacGillivray, H. T. 2001b, *MNRAS*, 326, 1295
- Hambly, N. C., et al. 2001c, *MNRAS*, 326, 1279
- Hogg, D. W., Eisenstein, D. J., Blanton, M. R., Bahcall, N. A., Brinkmann, J., Gunn, J. E., & Schneider, D. P. 2005, *ApJ*, 624, 54
- Huchra, J. P., Geller, M. J., Clemens, C. M., Tokarz, S. P., & Michel, A. 1996, *VizieR Online Data Catalog*, 7193, 0
- Huchra, J. P., et al. 2012, *ApJS*, 199, 26
- Ilbert, O., et al. 2006, *A&A*, 457, 841
- Jarrett, T. 2004, *PASA*, 21, 396
- Jarrett, T.-H., Chester, T., Cutri, R., Schneider, S., Rosenberg, J., Huchra, J. P., & Mader, J. 2000a, *AJ*, 120, 298
- Jarrett, T. H., Chester, T., Cutri, R., Schneider, S., Skrutskie, M., & Huchra, J. P. 2000b, *AJ*, 119, 2498
- Jarrett, T. H., et al. 2011, *ApJ*, 735, 112
- . 2013, *AJ*, 145, 6
- Johnston, S., et al. 2008, *Experimental Astronomy*, 22, 151
- Jones, D. H., et al. 2004, *MNRAS*, 355, 747
- . 2009, *MNRAS*, 399, 683
- Juzskiewicz, R., Vittorio, N., & Wyse, R. F. G. 1990, *ApJ*, 349, 408
- Kaiser, N., et al. 2002, in *Society of Photo-Optical Instrumentation Engineers (SPIE) Conference Series*, Vol. 4836, Society of Photo-Optical Instrumentation Engineers (SPIE) Conference Series, ed. J. A. Tyson & S. Wolff, 154–164
- Kashlinsky, A., Atrio-Barandela, F., Kocevski, D., & Ebeling, H. 2008, *ApJ*, 686, L49
- Keller, S. C., et al. 2007, *PASA*, 24, 1
- Kocevski, D. D., & Ebeling, H. 2006, *ApJ*, 645, 1043
- Kovács, A., Szapudi, I., Granett, B. R., & Frei, Z. 2013, *MNRAS*, 431, L28
- Kraan-Korteweg, R. C., & Jarrett, T. 2005, in *Astronomical Society of the Pacific Conference Series*, Vol. 329, *Nearby Large-Scale Structures and the Zone of Avoidance*, ed. A. P. Fairall & P. A. Woudt, 119
- Lahav, O., Kaiser, N., & Hoffman, Y. 1990, *ApJ*, 352, 448
- Laureijs, R., et al. 2012, in *Society of Photo-Optical Instrumentation Engineers (SPIE) Conference Series*, Vol. 8442
- Laurino, O., D’Abrusco, R., Longo, G., & Riccio, G. 2011, *MNRAS*, 418, 2165
- Lavaux, G., & Hudson, M. J. 2011, *MNRAS*, 416, 2840
- Lavaux, G., Tully, R. B., Mohayaee, R., & Colombi, S. 2010, *ApJ*, 709, 483
- Maller, A. H., McIntosh, D. H., Katz, N., & Weinberg, M. D. 2003, *ApJ*, 598, L1
- Marín-Franch, A., et al. 2012, in *Society of Photo-Optical Instrumentation Engineers (SPIE) Conference Series*, Vol. 8450, Society of Photo-Optical Instrumentation Engineers (SPIE) Conference Series
- Marinoni, C., Bel, J., & Buzzi, A. 2012, *JCAP*, 10, 36
- McMahon, R. 2012, in *Science from the Next Generation Imaging and Spectroscopic Surveys*
- Meisner, A., & Finkbeiner, D. P. 2013, in *American Astronomical Society Meeting Abstracts*, Vol. 221, American Astronomical Society Meeting Abstracts, #223.06
- Murakami, H., et al. 2007, *PASJ*, 59, 369
- Neugebauer, G., et al. 1984, *ApJ*, 278, L1
- Nusser, A., Branchini, E., & Davis, M. 2011, *ApJ*, 735, 77
- . 2012, *ApJ*, 744, 193
- Nusser, A., & Davis, M. 2011, *ApJ*, 736, 93
- Oyaizu, H., Lima, M., Cunha, C. E., Lin, H., & Frieman, J. 2008, *ApJ*, 689, 709
- Planck Collaboration et al. 2013a, *ArXiv e-prints*
- . 2013b, *ArXiv e-prints*
- Rassat, A., Land, K., Lahav, O., & Abdalla, F. B. 2007, *MNRAS*, 377, 1085
- Sachs, R. K., & Wolfe, A. M. 1967, *ApJ*, 147, 73
- Sarkar, P., Yadav, J., Pandey, B., & Bharadwaj, S. 2009, *MNRAS*, 399, L128
- Saunders, W., et al. 2000, *MNRAS*, 317, 55
- Schlafly, E. F., & Finkbeiner, D. P. 2011, *ApJ*, 737, 103

⁸ <http://www.ipac.caltech.edu/2mass/>

⁹ <http://wise.ssl.berkeley.edu/>

¹⁰ <http://surveys.roe.ac.uk/ssa/index.html>

¹¹ <http://www.sdss.org/>

¹² <http://www.gama-survey.org/>

- Schlegel, D. J., Finkbeiner, D. P., & Davis, M. 1998, *ApJ*, 500, 525
- Schröder, A. C., Mamon, G. A., Kraan-Korteweg, R. C., & Woudt, P. A. 2007, *A&A*, 466, 481
- Scrimgeour, M. I., et al. 2012, *MNRAS*, 425, 116
- Skrutskie, M. F., et al. 2006, *AJ*, 131, 1163
- Sunyaev, R. A., & Zeldovich, I. B. 1980, *MNRAS*, 190, 413
- Tagliaferri, R., Longo, G., Andreon, S., Capozziello, S., Donalek, C., & Giordano, G. 2003, *Lecture Notes in Computer Science*, 2859, 226
- Taylor, M. B. 2005, in *Astronomical Society of the Pacific Conference Series*, Vol. 347, *Astronomical Data Analysis Software and Systems XIV*, ed. P. Shopbell, M. Britton, & R. Ebert, 29
- Turnbull, S. J., Hudson, M. J., Feldman, H. A., Hicken, M., Kirshner, R. P., & Watkins, R. 2012, *MNRAS*, 420, 447
- Vanzella, E., et al. 2004, *A&A*, 423, 761
- Verheijen, M., Oosterloo, T., Heald, G., & van Cappellen, W. 2009, in *Panoramic Radio Astronomy: Wide-field 1-2 GHz Research on Galaxy Evolution*
- Wadadekar, Y. 2005, *PASP*, 117, 79
- Wang, D., Zhang, Y.-X., Liu, C., & Zhao, Y.-H. 2008, *ChJAA*, 8, 119
- Wang, T., Huang, J.-S., & Gu, Q.-S. 2009, *Research in Astronomy and Astrophysics*, 9, 390
- Way, M. J., Foster, L. V., Gazis, P. R., & Srivastava, A. N. 2009, *ApJ*, 706, 623
- Way, M. J., & Klose, C. D. 2012, *PASP*, 124, 274
- Way, M. J., & Srivastava, A. N. 2006, *ApJ*, 647, 102
- Woudt, P. A., Kraan-Korteweg, R. C., Lucey, J., Fairall, A. P., & Moore, S. A. W. 2008, *MNRAS*, 383, 445
- Wright, E. L., et al. 2010, *AJ*, 140, 1868
- Yuan, H. B., Liu, X. W., & Xiang, M. S. 2013, *MNRAS*, 430, 2188